MICHIGAN STATE UNIVERSITY LIBRARIES
3 1293 01579 6000

THESIS
2
(1995

This is to certify that the

dissertation entitled

A CRITERION TO PREDICT DAMAGE

IN ARTICULAR CARTILAGE DUE TO BLUNT IMPACT

presented by

Xiaowei Li

has been accepted towards fulfillment
of the requirements for

Ph.D. degree in Mechanics

Nicholas J Altiero

Major professor

Date February 20, 1995

MSU is an Affirmative Action/Equal Opportunity Institution O-12771

LIBRARY
Michigan State
University

PLACE IN RETURN BOX to remove this checkout from your record.
TO AVOID FINES return on or before date due.

DATE DUE	DATE DUE	DATE DUE

MSU Is An Affirmative Action/Equal Opportunity Institution
c:\circ\datedue.pm3-p.1

A CRITERION TO PREDICT DAMAGE IN ARTICULAR CARTILAGE DUE TO BLUNT IMPACT

By

Xiaowei Li

A DISSERTATION

Submitted to
Michigan State University
in partial fulfillment of the requirements
for the degree of

DOCTOR OF PHILOSOPHY

Department of Materials Science and Mechanics

1994

ABSTRACT

A CRITERION TO PREDICT DAMAGE IN ARTICULAR CARTILAGE DUE TO BLUNT IMPACT

By

Xiaowei Li

Excessive mechanical load to the knee during a blunt impact can initiate a degenerative disease process. Laboratory experiments have shown that the stresses and strains generated in the knee joint during impact can cause gross mechanical tissue damage. There are two basic types of damage reported in the knee joint under impact loading: fissures on the surface of the cartilage and/or microcracks in the subchondral bone or calcified cartilage. A mechanical damage criterion is developed in this dissertation using new experimental data, old observations and some new analytical results using the finite element method. A Coulomb-Mohr damage criterion is applied to study mechanics of biological tissue trauma. The failure envelop reveals that the damage of cartilage from the tibial plateau is controlled by two variables: shear stress and hydraulic pressure. In fact, the effect of static hydraulic pressure is significant and can not be ignored. The criterion is robust and can be used to help explain other types of biological tissue damage during blunt impact loading.

Dedication

To my parents: Zhou Li and L. Zheng. To my husband XianLi Huang and my daughters: SiRui and Rachel.

Acknowledgments

I would like to express my sincere appreciation to my advisors, Professor Nicholas J. Altiero and Professor Roger C. Haut for their guidance, friendship and assistance all the way through the dissertation and for their training on me in professional faith, skills and insights of engineering.

I would like to thank my committee members Professors D. Liu and D. Yen for their advice, comment and help during my studies.

I would like to thank the following people: Jane Walsh for her histological preparations, Tammy Haut for her processing the data base by FEM models, Jean Atkinson for her work with the animals and Bill Newberry for his logistic analysis.

This research has been supported by a grant from the Centers for Disease Control and Prevention (R494CCR-503607).

TABLE OF CONTENTS

LIST OF TABLES

LIST OF FIGURES

Chapter 1 Introduction

1.1 Osteoarthritis in Our Society

Arthritis in all its forms is perhaps the most prevalent cause of disability in the United States (Brown, 1988). Chronic disability caused by osteoarthritis (OA) is second only to that caused by cardiovascular disease. Diagnosis of this disease is primarily based upon radiographic assessment and clinical examination of the features (Altman, et al., 1986; and 1987). Although the states of this disease have been described in detail (Mankin, 1974), many questions still exist about its pathogenesis and the sequence of events leading to its formation. Traumatic joint injury has been speculated as a possible triggering mechanism for the onset of osteoarthritis. It has been hypothesized that articular cartilage damage sustained during impact may lead to altered joint loading and progressive degeneration (Repo and Finlay, 1977). While the mechanisms responsible for this disease are largely unknown, mechanical insult is speculated as one potential factor (Insall, 1976). A primary complication associated with lower extremity injury in motor vehicle accidents is post-traumatic osteoarthrosis (States, 1970). A direct association, however, between mechanical insult and the development of osteoarthritis has been difficult because radiographic evidence of the disease often does not show up for 2-5 years (Wright, 1990). On the other hand, only about 12% of patients with secondary osteoarthritis from a mechanical insult are free of pain in the interval immediately following the event (Chapchal, 1978).

Osteoarthritis (OA) is a degenerative disease which involves deterioration of the articular cartilage and subchondral bone (Meachim, and Brooke, 1984). This degeneration process is believed to result from a combination of mechanical loading and biological weakening of the cartilage matrix. An understanding of the mechanisms of

macro trauma to the structures and tissues of the knee requires a simple understanding of their normal function.

Articulating joints are the functional connections between different bones of the skeleton. In synovial, or freely moving joints, the articulating bone ends are covered with a soft white layer, a low friction gliding layer of connective tissue: the articular cartilage. The main functions of this articular cartilage are: (1) to spread loads to the joint so that it is transmitted over a large area, and the contact stresses are decreased and (2) to allow relative movement of the opposing surfaces with minimum friction and wear.

There are two main components in articular cartilage. The solid matrix of cartilage, which accounts for 20 to 40 % of the tissue's wet weight, is composed of collagen fibers. The remaining 80 to 60 % of the tissue is water, most of which can be squeezed out under load.

Since articular cartilage is highly resistant to fluid flow (i.e., low permeability), its material behavior is very much dependent on the rate at which the load is applied and removed. Thus in a rapid loading situation, when there is not time for the fluid to be squeezed out, the tissue will behave more or less like an elastic, single-phase material, deforming instantaneously upon loading and recovering instantaneously upon unloading. However, if the load is applied slowly to the tissue, as for example during prolonged standing, the deformation will continue to increase in time as the fluid is squeezed.

The two types of cartilage mechanical behavior described above are: time independent or elastic material behavior (the deformation may be recoverable); and time dependent or viscoelastic material behavior. A discussion of both materials of cartilage follow.

1.2 Nature of Impacted Articular Cartilage

Several impact models have been used to study the in vivo processes leading to the development of osteoarthritis. These models typically involve a single, concentrated blow to the test joint in order to inflict trauma. The trauma induced by transarticular impact can

be divided into two categories, based on the extent of the damage. These categories include (1) articular cartilage damage without disruption of the underlying bone or calcified cartilage and (2) subchondral bone fractures (often including damage to the overlying articular cartilage).

The type 1 defects are limited to the articular cartilage, do not involve the subchondral bone and do not elicit an acute inflammatory reaction (Glowacki, 1986; and Chueng, 1878). Acute fissures are a frequently reported form of impact damage to articular cartilage (Figure 1.1). These fissures most often begin at the surface and extend downward into the middle/deep zones of the cartilage (Repo, 1977; Broom, 1986; Haut, 1986; Thompson, 1990; Silyn-Roberts, 1990; Ide, 1990; Thompson, et al 1990; Tomatsu, 1992; Thompson, 1993). Repo and Finlay (1977) examined the response of human cartilage-on-bone samples under several levels of impact loading. They documented radial fissures in the center of the contact zone at the cartilage surface extending to the deep zone, and death of chondrocytes when average normal contact pressures reached 25 MPa. Silyn-Roberts, et al, (1990) reported that impact induced failures of cartilage, in vivo, were usually in the center of the contact zone and oriented at 45 degrees to the articular surface and extended into the mid-zone.

The type 2 defects penetrate the subchondral bone and participate an inflammatory response and the attempted regeneration of the tissue (Glowaki, 1986; Pritzker, 1991; and Bland, 1983). The fractures in the calcified cartilage and subchondral bone are often seen in conjunction with fissures that extend up into the cartilage, but do not reach the articular surface (Thompson, 1991; Vener, 1992). Using a rabbit model and cyclic impulse loading, Radin (1973, 1978, 1984)) was able to measure an increase in the subchondral bone stiffness as well as progressive decreases in the proteoglycan content of cartilage in the traumatized knee(Figure 1.2). Separation of the cartilage from the underlying bone in the zone of calcified cartilage has also been reported in response to blunt impact (Armstrong, et al, 1982). Vener, et al, (1991) have observed cracks in the zone of

calcified cartilage after impact of canine joints. In a more recent study, increased bone volume was reported to have a correlation with the severity of osteoarthritis observed in human articular cartilage (Shimizu, 1993). The results of studies such as these have prompted many investigators to believe that osteoarthritis is mediated by initial changes in the subchondral bone.

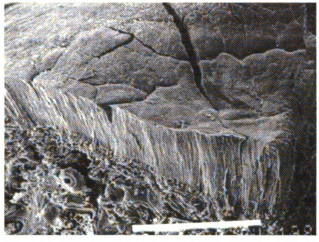

Figure 1.1 Surface fissures extend deeply into the radial zone in the rabbit tibial plateau.

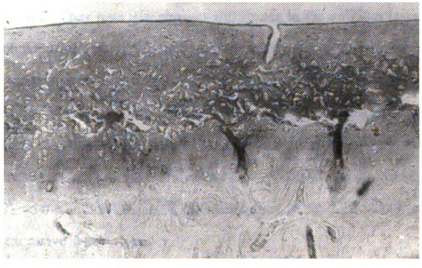

Figure 1.2 Horizontal splitting at the tidemark was frequent in tibial cartilage from the experiments (Radin, at. al. , 1984).

1.3 Mechanics Models

Many researchers believe that fissuring of the articular surface ultimately leads to the development of osteoarthritis. A few different mechanics models have been developed to address the impact contact problem that yields these fissures.

Askew and Mow (1978), using elastic models subjected to impact profiles, argued that tensile strains, rather than stresses, may be a more reliable predictor of where fissures are likely to form. The model predicted large shear stresses at the cartilage and bone interface, which may account for separations seen experimentally (Askew and Mow, 1978; Chin, 1986). Eberhardt, et al (1990) modeled joint contact as a layered elastic sphere against a layered elastic cavity. They discussed the effects of cartilage thickness and stiffness, bone stiffness and curvature on the distribution of stresses in cartilage and the underlying bone. A later study (Eberhardt, et al, 1991) utilized a solution based on normal contact of two elastic spheres. The authors suggested that cartilage stresses are not significantly affected by stiffness of the underlying bone. Tensile radial strains in the cartilage approach one-third the normal compressive strains, and increase with softening of the cartilage. The model by Askew and Mow (1978) bonds the elastic layer to a high modulus half-space of subchondral bone and introduces a parabolically distributed pressure to the surface. They note that stresses and strains in the articular layer strongly depend on the contact aspect ratio. The also documented large tensile strains parallel to the surface near the center of the loading area. Armstrong, C. G., et al (1984) indicated this coincides with the area where cartilage delaminates during blunt impact experiments . Large tensile strains also develop in the cartilage near the location of surface fissures (Haut, 1992). These fissures are typically oriented at 45 degrees to the surface (Silyn-Roberts, H. 1990), so the authors suggest that tissue failure in the zone of compression is primarily due to excessive shear stress.

G. A. Ateshian (1994) performed an analysis of cartilage based on its biphasic material behavior. This analysis provides strong support for the hypothesis that, if sudden

loading causes shear failure within the cartilage-bone layer structure, failure would take place at the cartilage-bone interface, and the plane of failure would be either parallel or perpendicular to this interface.

1.4 Statement of the Problem

The degree of mechanical damage to a knee under impact loading initiates a degenerative disease process. There are many factors affecting degenerative process. It has been shown by experiments that the stresses and strains generated in the knee joint cause fissures on the cartilage surface and cracks in the bones. The damage mechanism of tissue trauma leading to osteoarthritis is not yet fully understood, even though there have been a large number of contributions to this field of study. There are two types of damage in the knee joint under impact loading shown by experiments: fissures occurring on the surface of the cartilage, and cracks in the subchondral bone or calcified cartilage. The question arises: what causes these fissures and cracks? To answer this question, a quantitative analysis is required to determine which factors cause the damage and a quantitative damage criterion is needed to predict tissue damage. A quantitative analysis of the tissue fissures and cracks can be accomplished by a finite element model of the knee joint to simulate the damage process.

Chapter 2 Background and Objectives

A lot of experimental data will be needed to develop a quantitative damage criterion. The experimental data and observations from impacted knee joints of rabbits performed by Ide (1992), will be used in this dissertation. It will be necessary to review these experimental results. Furthermore, a damage criterion will be developed in this dissertation on the basis of a quantitative analysis of these data and relevant damage theories. Damage theories and their application to tissue injury mechanisms will be reviewed.

2.1 Experimental Results for Impact of Rabbit Knee Joints

Alterations in the mechanical properties of the rabbit's patellar cartilage were measured with a single blunt impact (Haut et al, 1992). The impacts were delivered to the flexed hind limb of thirty-four anesthetized Flemish Giant rabbits. The patellar cartilage of the rabbit was traumatized at one of the energy levels: 0.9J, 4.2J, or 6.3 J. Contact pressure distributions were recorded in the patello-femoral joint with Fuji Prescale film (Figure 2.1). The peak contact pressures over the lateral patellar facet statistically exceeded those over the medial facet by approximately 8 MPa (Figure 2.2). The experimental study indicated that the existence of a biomodal distribution in the contact pressures had a strong correlation with cartilage damage. The correlation of fissuring with the magnitude of the average contact pressure, per se, is shown in Figure 2.3.

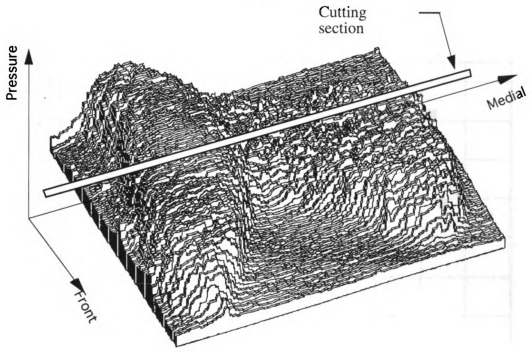

Figure 2.1 A Typical distribution of contact pressure recorded on Fuji Film by impact

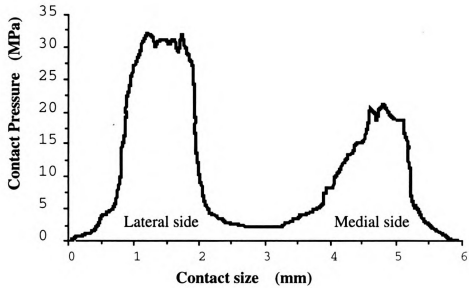

Figure 2.2 The profile of contact pressure in the cut section

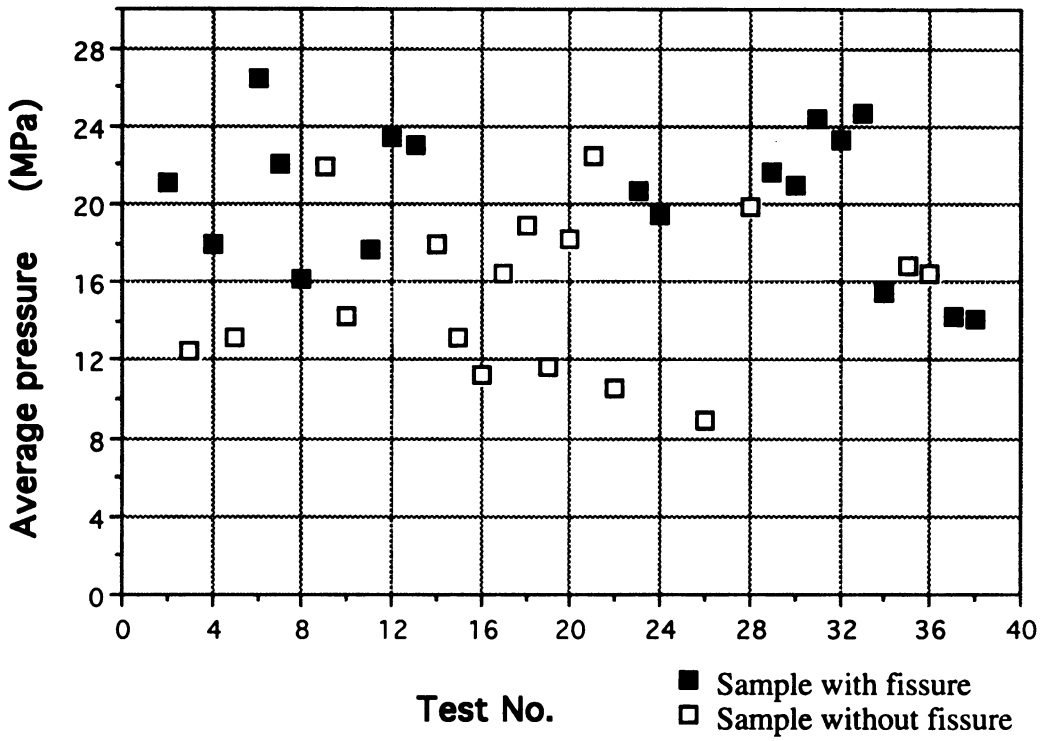

Figure 2.3 Average pressures data from 34 impact experiments (Ide, 1992)

Another important experimental observation was that fissures in the cartilage layer were oriented longitudinally on the lateral facet. The fissures were generally located at the periphery of the lateral contact zone nearest to the center line (Figure 2.4 a). Histological sections (Haut, 1992 and 1991) showed that the fissures follow the line of chondrocytes (cells), orienting themselves parallel to the major collagen bundles in the cartilage layer (Figure 2.4 (b)).

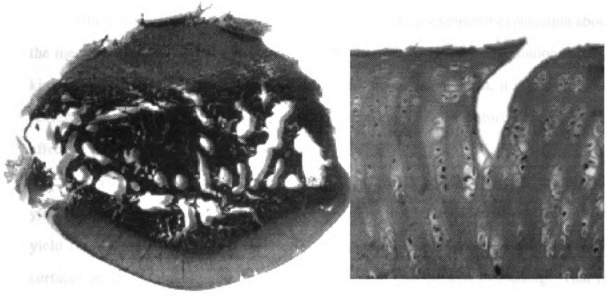

(a) (b)

Figure 2.4 Fissure location in the impacted cartilage and its orientation

These experimental data and subsequent observations gave us important information needed to help understand injury to soft tissue by blunt impact, even though the results only show a rough relationship of damage to contact pressure. In this dissertation, the stress fields from Ide's experimental data will be estimated by a patella FEM model. The damage of cartilage, i.e. fissures, and its correlated stresses obtained by the FEM model will be further analyzed using based on engineering damage criteria. Although a number of criteria have been applied to normal engineering materials, none to date have been applied to biological tissues.

2.2 Candidate Failure Criteria

Starting from these experimental data I will provide a reasonable explanation about the mechanics of damage and develop a failure criterion to give an explanation for this kind of impact trauma. In order to explain these damage phenomena, it is necessary to review the existing failure criteria in engineering applications before developing an effective criterion for knee joint damage.

1. The Tresca criterion, also known as the maximum shear theory, states that yielding of an isotropic material will begin when the maximum shear stress reaches the yield limit for the material. This theory is suggested by the observation that failure surfaces in ductile materials in static tension are at 45° to the axis of loading. That is, failure surfaces are planes that carry maximum shear stress. The Tresca criterion can be written as:

$$\tau_{max} \leq \tau_s \tag{2.1}$$

where τ_{max} is the maximum shear stress, and τ_s is a constant related to material yield.

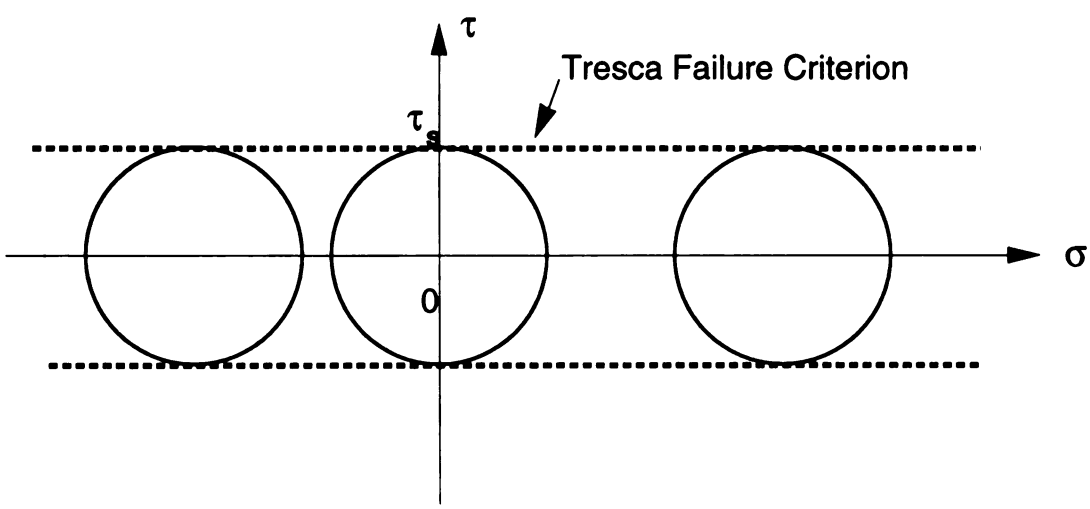

Figure 2.5 The Tresca failure criterion

This criterion has been applied to engineering materials that fail by yielding, such as metals and alloys.

2. The Von Mises criterion states that yielding of an isotropic material will begin when the effective stress reaches the yield limit for the material. The Von Mises criterion can be written:

$$\sigma^* = \sqrt{\sigma_x{}^2 + \sigma_y{}^2 + \sigma_z{}^2 - \sigma_x\sigma_y - \sigma_y\sigma_z - \sigma_z\sigma_x + 3(\tau_{xy}{}^2 + \tau_{yz}{}^2 + \tau_{zx}{}^2)} \leq \sigma_s \qquad (2.2)$$

where σ^* is the effective stress and σ_s is the yield constant for the material in unaxial tension. Equation (2.2) can be written in another form in terms of the principal stresses:

$$\sigma^* = \sqrt{\frac{1}{2}\{(\sigma_1 - \sigma_2)^2 + (\sigma_2 - \sigma_3)^2 + (\sigma_3 - \sigma_1)^2\}} \leq \sigma_s \qquad (2.3)$$

From equation (2.3) it is clear that the effective yield stress is not affected by the level of hydraulic pressure in the material.

This criterion has been applied to engineering materials which fail by yielding, such as metals and alloys. The Von Mises criterion gives a more accurate analysis of failure than does the Tresca criterion for many engineering applications.

3. The maximum principal strain criterion states that tensile fracture surfaces will form in previously uncracked isotropic materials when the maximum principal strain reaches a limiting value in tension.

$$\varepsilon_{max} \leq \varepsilon_{limit} \qquad (2.4)$$

where ε_{max} is the maximum tensile strain, ε_{limit} is the limiting constant value of material in tension. This criterion is usually applied to brittle engineering materials in tension. These often fail by fracture and not by yielding. Glass is one type of material that fails by this mechanism..

4. Mohr criterion states that failure of an isotropic material, either by fracture or by the onset of yielding, will occur when the largest Mohr circle (having a diameter determined by the difference between the maximum principal stress and the minimum

principal stress) reaches a failure envelop. Experiments show that the envelop, which is tangent to all the failure circles and bounds the safe region, is usually curved convex outward.

This criterion is usually applied to some brittle engineering materials in compression, which fail by fracture, instead of yielding. Rock, cast metal, soil, brick and concrete are typical examples. Such materials exhibit a compressive strength that is much higher than the tensile strength. The media is usually discontinuous with a lot of voids and flaws, or micro cracks. Cartilage and bone have this kind of characters and typically function under high levels of compression, especially during blunt impact. Furthermore, the compressive strength of these tissues is more than two times higher than the tensile strength (H. Yamada, 1970). Thus, a Mohr criterion is considered in this study. A more detailed discussion of this failure criterion will be given below.

Mohr proposed a criterion of the form

$$|\tau| = f(\sigma_n) \tag{2.5}$$

Where τ and σ_n are the shear stress and the normal stress on the failure plane, and $f(\sigma_n)$is the failure function for the envelop. The failure envelop for a Mohr criterion can be determined experimentally from a series of triaxial compression tests. This criterion includes the effect of hydraulic pressure. Mohr theory is usually used for brittle materials, which are much stronger in compression than in tension. When compression is dominant, failure occurs along shear planes inclined at an angle of $45^{o}+1/2\phi$ to the direction of minimum principal stress (Figure 2.6). Mohr circle describing the state of stress at fracture is plotted for each test. The function $f(\sigma_n)$ is then defined by the envelop which is tangent to the set of these Mohr circles. The failure envelop function $f(\sigma_n)$, which is called Mohr criterion, is usually non-linear (Figure 2.6).

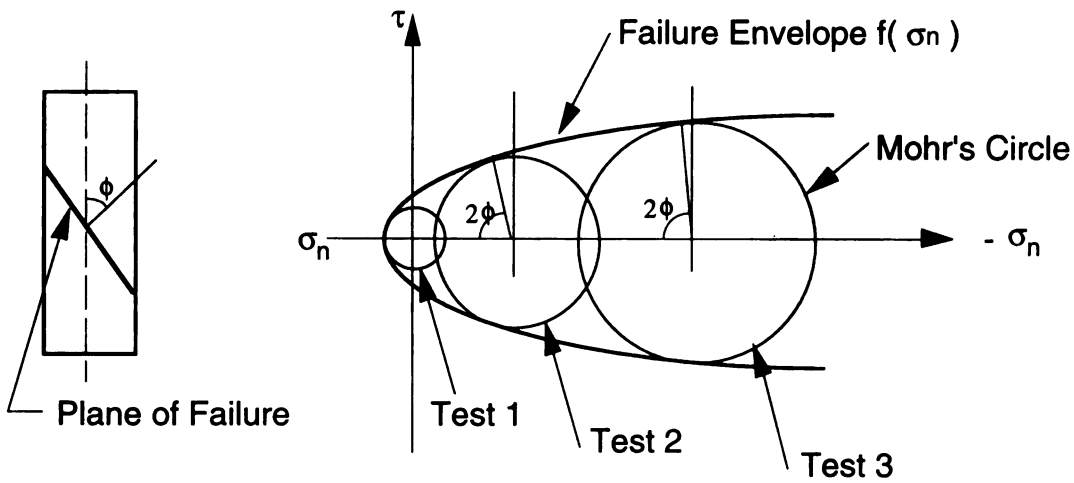

Figure 2.6 The failure criterion of Mohr

A failure criterion due to Coulomb in 1776 states that fracture or damage occurs in a solid body when shear stresses on some plane in that body are large enough to overcome the sum of the "cohesive strength", C, and the frictional stress, $-\mu\sigma_n$, caused by the normal stress on that plane σ_n (Figure 2.7). The failure envelop, which is called the Coulomb-Mohr Criterion, is linear and can be written as:

$$\tau = C + \mu\sigma_n \tag{2.6}$$

where C is the intrinsic shear strength of the material (cohesion) and σ_n is the normal stress on the plane, $\mu = \tan\phi$, ϕ is the angle of internal friction, and τ is the shear stress.

A simple way to approximate the envelop of Equation (2.6) is to draw a pair of straight lines tangent to two Mohr circles (Figure 2.8). One circle represents the ultimate uniaxial tensile stress, and the other represents ultimate uniaxial compressive stress. The materials constants C and μ can be determined from curve fitting, based on these two Mohr circles.

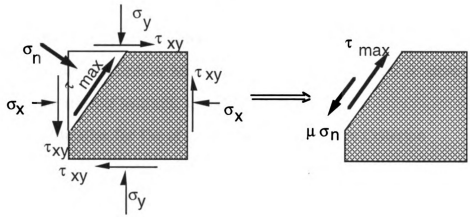

Figure 2.7 The model of Coulomb-Mohr

With a straight-line envelop, the Coulomb-Mohr theory is also known as the internal-friction theory because it can be derived by accounting for friction along slip planes. The Coulomb-Mohr criterion specifies maximum shear stress on any plane. That is, the resistance to failure of a material is a constant shear strength plus a friction-like force, $\mu\sigma_n$ (Figure 2.7).

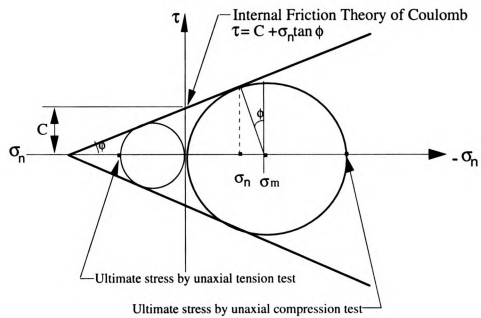

Figure 2.8 The failure criterion of Coulomb

Unlike the one-parameter failure model (Tresca criterion or maximum strain failure criterion), the Coulomb or Mohr failure theories include two or more material parameters and the effect of hydraulic stress on material failure.

2.3 Physical Justification for Use of a Coulomb-Mohr Failure Criterion

Several theoretical studies have addressed the problem of determining the stress and strain fields in a cartilage layer in order to explain the remarkable longlasting quality of this tissue, as well as to identify those mechanical factors which may lead to cartilage degeneration. However, applicable damage criterion have not been well studied.

There are several reasons why a Coulomb-Mohr failure criterion may be applied to articular cartilage. First, articular cartilage is a discontinuous material with a lot of micro flaws, voids, and fibers. When high normal pressures act on these flaws, the frictional resistance reduces shear stresses and helps resist micro crack growth. The cartilage in the knee joint, typically withstands high hydraulic pressures. The convex and concave curvature contact surfaces contain this soft tissue so as to bear high pressures under short time loading. The fluid phase of cartilage does not have time to move out and therefore shares a significant percentage of load (Ateshion et. al, 1994).

Second, the damage phenomenon in cartilage is similar to that of brittle materials. There are a lot of microcracks and fiber debonding before fissures actually form. Surface images of non damaged and damaged areas scanned by electronic microscopy are shown in Figures 2.9 (a) and 2.9 (b), respectively. Comparing these two pictures, we can see that the distribution of fibers is nearly uniform in the non damaged zone and there is a zone of micro-cracks along the crack tip in the damage zone. Clark (1971) also showed that many micro cracks occur before a fissure grows. The network of fibers is strong in tension, but the matrix of soft tissue is very easily damaged by shear deformation.

Third, the loading rate can change a material's behavior from ductile to brittle, particularly if the material is under hydraulic compression. Brittle materials initially failed

by many micro-cracking (Altiero, 1974), and then failure by macro-crack growth occurs (Figure 2.10). The resistance to shear deformation increases with an increase in level of hydraulic stress. However, the 'failure surface' in such conditions depends not only on the deviation (shear) stresses, as in the Von Mises law, but also on the magnitude of the average compressive stress.

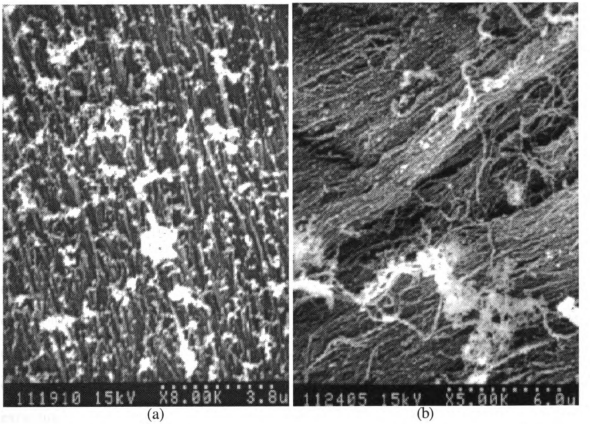

(a) (b)

Figure 2.9 (a) Scanning a section of cartilage (b) Scanning a section of the damage zone on the impacted sample from a rabbit

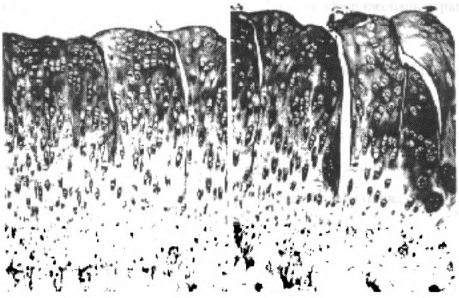

Figure 2.10 Fissure growth in the soft tissue along collagen fibers

2.4 The Study Objectives

The exact mechanism of impact induced cartilage fissuring is not known. A number of predictive parameters for articular cartilage failure have been proposed. The common factors in these proposals and associated models have not been proved by experiments, so they have not given a quantitative analysis for establishing a damage criterion for bio-tissue under impact. The objective of this dissertation is to conduct experiments and develop a theoretical model to help understand the physics behind the development of cartilage fissures during blunt impact. This development of a criterion for the impact-induced micro damage of articular cartilage has involved in several stages.

(1) A finite element model of the knee joint was employed to estimate the unknown material properties of cartilage under impact by correlation with the experimental data using an inverse approach.

(2) Data from knee joint impact experiments (Ide, 1992) were then input into the FEM model to analyze the stress fields in the impacted knee joints. The results of the stress analyses were compared with Ide's experimental observations to develop a damage

criterion. A logistic regression analysis was used to find out which mechanical parameters best predicted cartilage damage.

(3) Since the regression analysis indicated that a combination of two variables (shear and mean stress) best predicted damage, a Coulomb-Mohr criterion was employed. The material properties needed for an effective failure criterion were then determined in independent experiments. The rabbit tibial plateau are flatter and have a better quality cartilage than do the patella, so they were used in this experimental tissue.

(4) The failure criterion was then applied to the earlier data of Ide. It is shown in that this dissertation that this new tissue failure criterion predicts the onset of surface fissures in the rabbit knee joint well.

Chapter 3 Computational Modeling Assumptions

Computational models of rabbit knee joints can quantitatively generate the stress and strain fields under impact loading. The stress and strain fields can then help determine relevant variables around fissure locations. The computational models require the material constitutive relations, the geometry of the joint, and impact loading conditions. For simplicity of the computational models, some assumptions were made and they are explained below.

3.1 Linear Elastic Behavior of Cartilage and Bone

The mechanical behavior of cartilage is very complicated and time dependent, particularly as related to free fluid flow under loading. Mow and his colleagues developed a biphasic continuum description to model the behavior of cartilage (Mow, et al, 1980). Others have applied a single phase viscoelastic model to describe the material response (Parsons, and Black, 1977). In this previous work, the attention has largely been focused on relatively long time scales. Our experiments are conducted under loading in a short time. Under this test condition, the fluid in the cartilage may not have time to move. Therefore, it may be reasonable to assume elastic behavior. We show that the available data support the use of an elastic behavior at rapid loading rates, and the effect of time dependence can be ignored in the following. The two typical solutions of cartilage constitutive models, viscoelastic and biphasic, are now compared to those of the elastic model.

Viscoelastic Model

Simon and his colleagues (1984) presented cartilage as a viscoelastic material. The normalized relaxation function $G^*(t)$ is given in the following form.

$$G^*(t) = 0.23 + 0.77e^{-0.92t} \tag{3.1}$$

The function $G^*(t)$ in equation (3.1) allows one to determine the normalized stress history, $\sigma^*(t)$, for any prescribed strain history by a hereditary integral formulation (Fung, 1965)

$$\sigma^*(t) = \int_0^t G^*(t-\tau)\frac{d\varepsilon(\tau)}{d\tau}d\tau \tag{3.2}$$

where $\varepsilon(t)$ is the prescribed time-dependent strain. For a constant strain rate:

$$\varepsilon(t) = \frac{\varepsilon_0 t}{T_a} \tag{3.3}$$

where T_a is the time of load application. Substituting (3.1) and (3.3) into (3.2) and integrating yields the normalized stress

$$\sigma^*(t) = \frac{\varepsilon_o}{T_o}\left[0.23t + 0.84\left(1 - e^{-0.92t}\right)\right] \tag{3.4}$$

Taking a Taylor expansion and ignoring higher order terms yields an approximate expression for the normalized stress:

$$\sigma^*(t) = [1.0 - 0.3542t](\frac{\varepsilon_0 t}{T_a}) \tag{3.5}$$

It can be seen from (3.5) that the viscoelastic solution consists of two terms. The first term is the elastic solution and the second term is the viscous effects. It indicates that when the loading period of application is small the solution is approximately an elastic solutions and when the loading period of application is long the viscoelastic solution dominates.

Biphasic Model

The stress expression history for a cylindrical biphasic material in unconfined compression was derived by Armstrong, (1984). For $t \rightarrow 0$, the normalized relaxation

function, $G^*(t)$ can be written as

$$G^*(t) = 1 - \frac{4\mu_s^2}{3H_A}\sqrt{\frac{H_A kt}{\pi a^2}} + O(t) \tag{3.6}$$

If the higher order terms, O(t), are neglected, $G^*(t)$ becomes:

$$G^*(t) = 1 - \frac{4\mu_s^2}{3H_A}\sqrt{\frac{H_A kt}{\pi a^2}} \tag{3.7}$$

where k is the permeability of the material, a is the radius of the specimen, μ_S is the shear modulus of the solid matrix and H_A is the aggregate modulus. H_A and μ_S can be expressed as follows:

$$H_A = E_s \frac{(1-\nu_s)}{(1+\nu_s)(1-2\nu_s)} \tag{3.7 a}$$

$$\mu_s = \frac{E_s}{2(1+\nu_s)} \tag{3.7 b}$$

where E_s and ν_s is Young's modulus and Poisson's ratio of the solid matrix, respectively. Substituting the following values into equations (3.7 a and b): E_s=0.7 MPa and ν_s=0.45 and 0.0, respectively, H_A and μ_s can be calculated and are listed in Table 3.1.

Table 3.1 Material properties of cartilage in biphasic model (Armstrong, et al, 1984)

	ν_s=0.45	ν_s=0.0
H_A (MPa)	2.66	0.70
μ_s (MPa)	0.24	0.35

Substituting these values of H_A, μ_s, k=0.2x10^{-14} m^4 / Nsm, and a=3.17 mm into equation (3.7) yields the expressions for $G^*(t)$.

The function $G^*(t)$ in equation (3.7) allows one to determine the normalized stress history, $\sigma^*(t)$, for any prescribed strain history by a hereditary integral formulation using equation (3.2). Substituting $G^*(t)$ into equation (3.2) and integrating, the normalized stress expressions of the biphasic model can be obtained:

$$\sigma^*(t) = [1.0 - 0.00104(t)^{\frac{1}{2}}](\frac{\varepsilon_0 t}{T_a}) \qquad \text{for } \nu_s=0.45 \tag{3.8}$$

$$\sigma^*(t) = [1.0 - 0.0030(t)^{\frac{1}{2}}](\frac{\varepsilon_0 t}{T_a}) \qquad \text{for } \nu_s=0.0 \tag{3.9}$$

The values of $\frac{\sigma^* T_a}{\varepsilon_o t}$ determined using equations (3.8), (3.9) and (3.5) are given in Table 3.2 for various times.

Table 3.2 Comparison of $\sigma^* T_a/\varepsilon_o t$ of the elastic solution to the viscoelastic and biphasic solutions

	Equation #	t=5 (ms)	t=50 (ms)	t=200 (ms)
Armstrong ν_s=0.45	(3.8)	0.9999	0.9997	0.9995
Armstrong ν_s=0.0	(3.9)	0.9998	0.9993	0.9986
Simon	(3.5)	0.9980	0.9820	0.9290

It can be seen from Table 3.2 that both models deviate from the elastic model by a very small amount within a loading time of 50 ms. The biphasic model stress varies from the elastic by 0.07 % at 50 ms. The viscoelastic model variation is 1.8 % at 50 ms. Therefore, the elastic constitutive law can be used for our model, since our impact loading time is less than 20 ms.

3.2 Justification for the Assumption of a Quasi-Static Load

A quasi-static state solution implies the use of a static solution to approximate a dynamic model. Since our experiments involve the free dropping of indenters on the knee joint, dynamic modeling would be appropriate. However, in this section, justification for a quasi-static approximation is examined. It is proposed that tensile stress waves occur only if the impulse load rate is larger than the speed of tensile wave propagation. In our impact model, stress wave propagation can be ignored. The simple proof of this impact model is presented in the following section.

Quasi-static State Solution

The total impact load, including indenter weight and dynamic load by acceleration, is input into our finite element model of the knee joint. It is equivalent to applying a d'Alembert force to a static-analysis model if the stress wave propagation is ignored. The equilibrium statement, written as the virtual work principle, is

$$\int_V \sigma:\delta D dV = \int_S t^T.\delta v dS + \int_V f^T.\delta v dV \tag{3.10}$$

where σ is the stress tensor, δD is the virtual strain rate tensor, t^T is a surface force vector, f^T is a body force vector, δv is the virtual velocity of deformation, V is the body volume and S is the body surface.

The body force at a point, f^T, can be written as the resultant of the externally prescribed body force, F and a d'Alembert force as follows.

$$f = F - \rho\ddot{u} \tag{3.11}$$

where ρ is the current density of the material at this point and $\ddot{u}$ is the acceleration at the point. Inserting the body force term into the virtual work, equation (3.10) becomes:

$$\int_V \sigma:\delta D dV = \int_S t^T.\delta v dS + \int_V (F - \rho\ddot{u})^T.\delta v dV \tag{3.12}$$

If wave propagation is neglected, equation (3.12) represents the quasi-static state solution.

The Effect of Stress Wave Propagation

Sudden loading to the knee joint or the cartilage surface of tibial plateau by impact is essentially a dynamic problem. When the load is first applied, its action is not transmitted instantaneously to all parts of the body. Waves of stress and deformation radiate from the loaded region with finite velocities of propagation. Let us consider a simple one-dimensional discontinuous-medium model, as shown in Figure 3.1.

In a simple one-dimensional discontinuous-medium model, the velocities of longitudinal wave propagation in medium 1 and medium 2, i.e., c_i i=1, 2, are given by Clove (1975):

$$c_i = \sqrt{\frac{E_i}{\rho_i}} \qquad \text{i=1, 2} \tag{3.13}$$

where E_i and ρ_i are Young's modulus and the density of the ith medium, respectively.

The reflected force, N_b, and the refracted force, N_c, can be expressed as fractions of the input force, N_a, at the interface of medium 1 and medium 2 (Clove (1975)):

$$N_b = N_a \frac{\alpha - 1}{\alpha + 1} \tag{3.14}$$

$$N_c = N_a \frac{2\alpha}{\alpha + 1} \tag{3.15}$$

where α is the following material constant :

$$\alpha = \frac{\sqrt{\rho_2 E_2}}{\sqrt{\rho_1 E_1}} \tag{3.16}$$

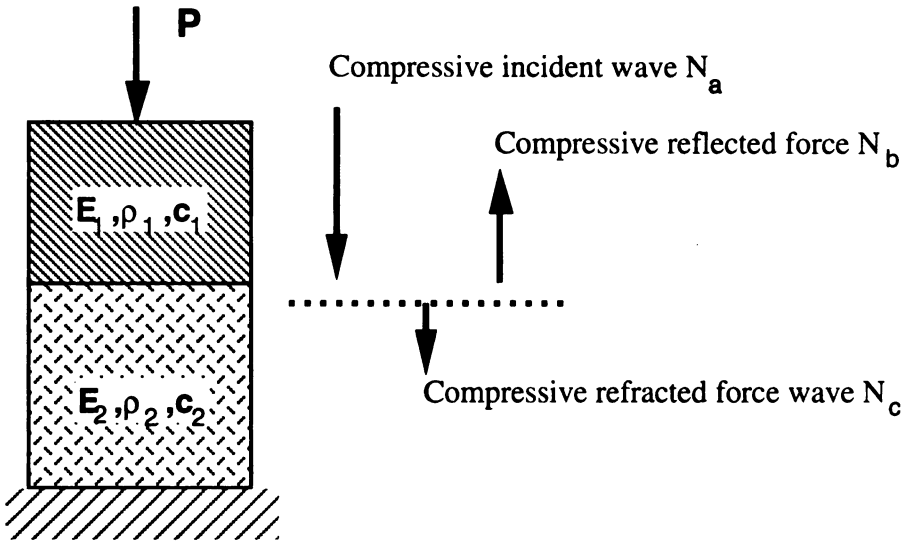

Figure 3.1 Forces at the interface in a one dimensional discontinuous medium

In this study, the Young's modulus and density of bone were obtained from S. C. Cowin (1987), and the properties of cartilage are based on estimations made in Chapter 4 of this dissertation. These properties are given in Table 3.3.

Table 3.3 Material properties of rabbit cartilage and bone

Material	E_i (N/m^2)	ρ_i (kg/m^3)
Cartilage	2×10^6	0.8×10^6
Bone	2×10^9	1.8×10^6

Now let us apply this one-dimensional wave propagation model to two possibilities: (1) impact load transmission at the interface from cartilage to bone (similar to our indenter impact test of tibial plateau), and (2) impact load transmission at the interface from bone to cartilage (similar to our impact test of knee joint).

Let medium 1 be cartilage and medium 2 be bone (Figure 3.2 (a)). Using the material properties given in Table 3.3 yields α=47.34 by Equation (3.16). The first

reflected force, N_b^1, can be obtained by Equation (3.14) and is equal to 0.954 N_a^1, and the first refracted force, N_c^1, can be obtained by Equation (3.15) and is equal to 1.954 N_a^1. Both N_b^1 and N_c^1 have the same sign as the input load, N_a^1 (i.e., they are compression forces).

Now let us calculate the first reflected force transmitted back to the cartilage surface. In this case, the input load, N_a^2, is equal to N_b^1. Let medium 1 be cartilage and medium 2 be air (Figure 3.2 (b)). The Young's modulus of air is 0, so the second reflected force at the cartilage surface, N_b^2, can be obtained by Equation (3.14) and is equal to - N_b^1. The refracted force, N_c^2, can be obtained by Equation (3.15) and is equal to 0.

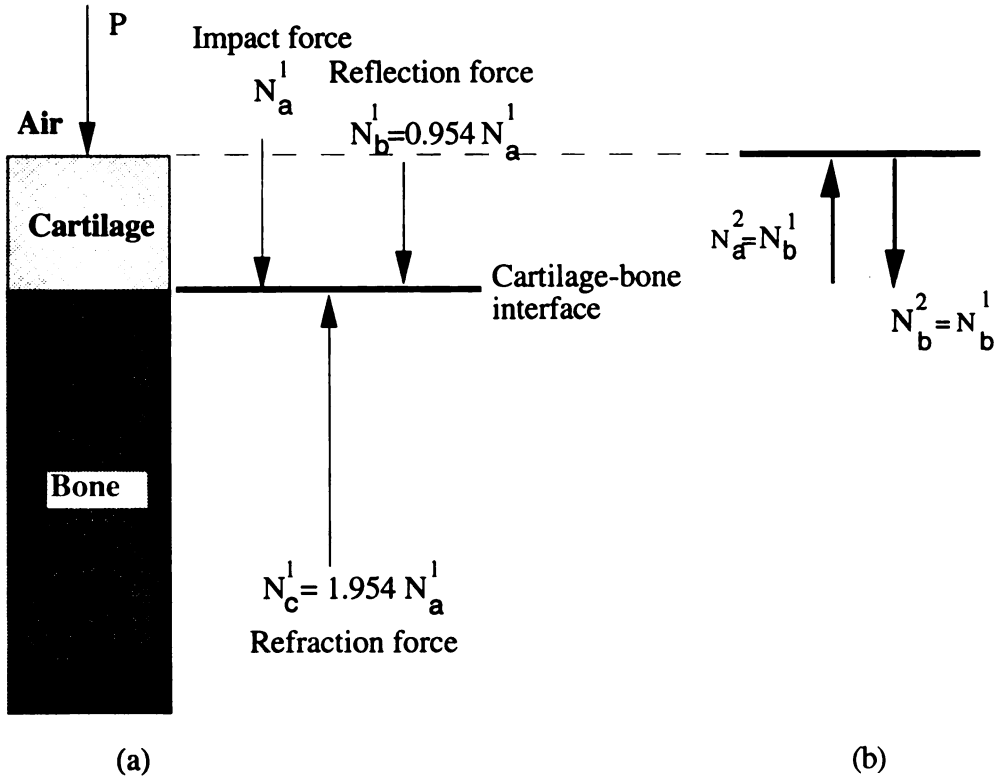

Figure 3.2 (a) Stress wave propagation from cartilage to bone. (b) Stress wave propagation from cartilage to cartilage surface

We can repeat the calculation to determine subsequent wave magnitudes of the

reflected force at the cartilage to bone interface. These magnitudes are shown in Figure 3.3.

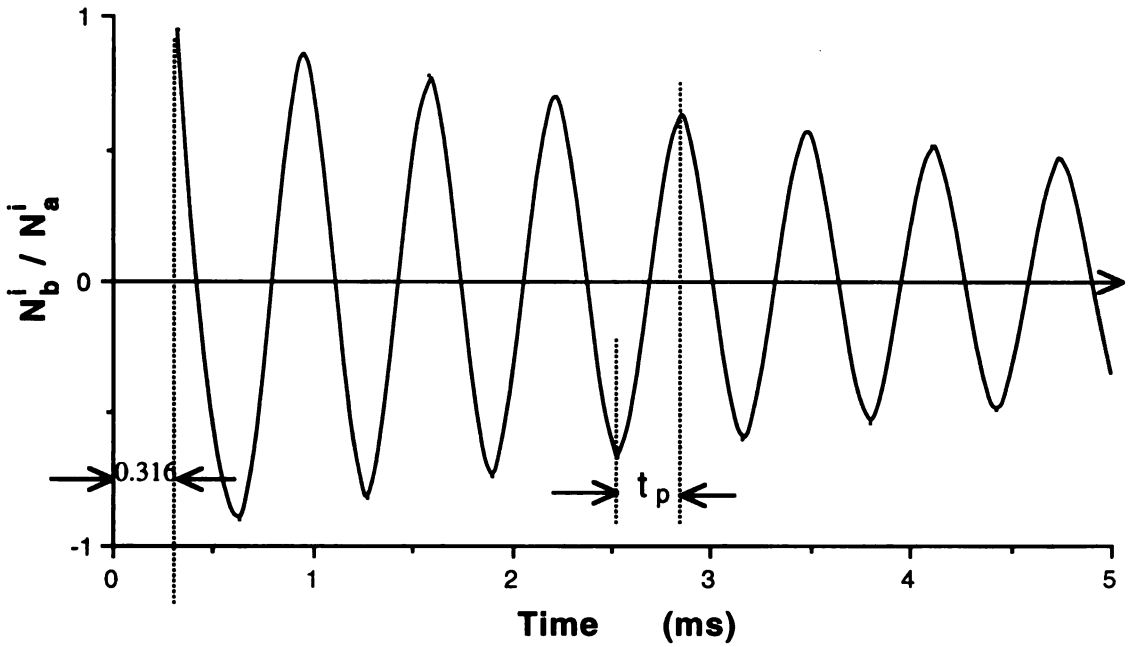

Figure 3.3 Reflected force at the cartilage-bone interface vs. time

The wave propagation velocity in the cartilage can be calculated using equation (3.13) and is equal to 1.58 mm/ms. If the thickness of cartilage is 0.5 mm, the time of wave propagation through the cartilage to the interface, t_p, can be simply calculated by dividing the bone thickness by wave velocity, c_1. Thus, t_p is equal to 0.316 ms/per half wave. Thus N_a^1 is equal to the value of the impact load at t=0.316 ms (Figure 3.4).

The results of the curve of experimental impact load vs. time and reflected force at the cartilage-bone interface are shown in Figure 3.4. The magnitude of stress wave is 6.6 % of the peak impact load. We have neglected damping of the material in this calculation and thus our estimates are liberal.

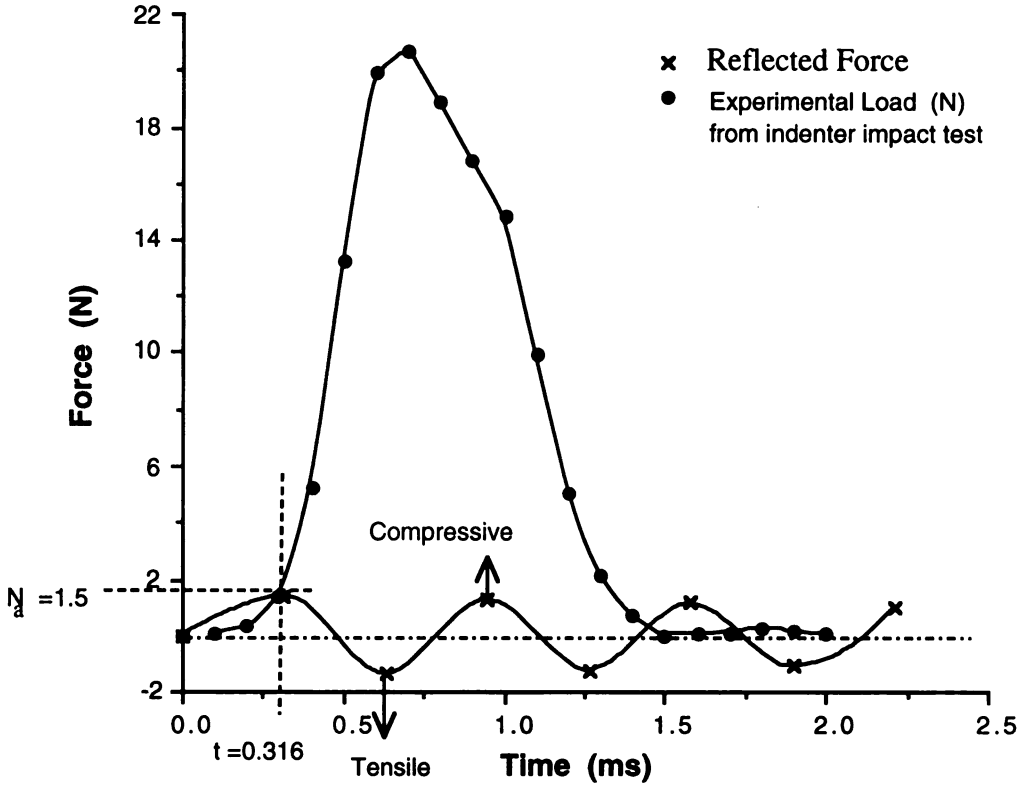

Figure 3.4 The effect of the reflected force on experimental impact load (cartilage to bone).

Let us now examine the second case. Let mediums 1 be bone and medium 2 be cartilage (Figure 3.5). Using the material properties given in Table 3.3, α=0.024 by Equation (3.16). The refracted force, N_c^1 , can be obtained by Equation (3.15) and is equal to 0.046 N_a^1, and the reflected force, N_b^1, can be obtained by Equation (3.14) and is equal to -0.954 N_a^1 . Note that the negative sign of the reflected force means the opposite of the sign of the input force. So, in this case, there exists a tensile reflected stress wave at the bone-cartilage interface. These forces are shown in Figure 3.5 .

Now, let us calculate the first reflected force transmitted back to the bone surface. In this case, the input load, N_a^2, is equal to N_b^1. Let medium 1 be bone and medium 2 be air (Figure 3.5 (b)). The Young's modulus of air is 0, so the second reflected force at the

bone surface, N_b^2, can be obtained by Equation (3.14) and is equal to - N_b^1. The refracted force, N_c^2, can be obtained by Equation (3.15) and is equal to 0.

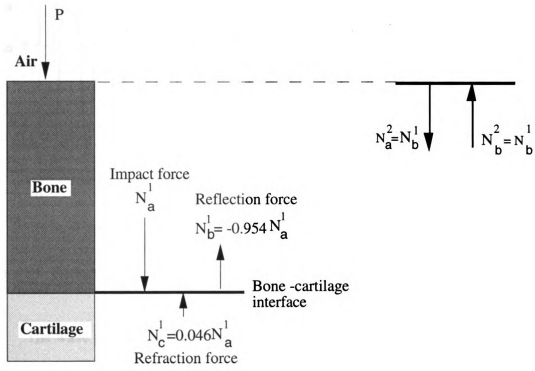

Figure 3.5 (a) Stress wave propagation from bone to cartilage. (b) Stress wave propagation from bone to bone surface.

We can repeat the calculation to determine subsequent wave magnitudes of the reflected force at the bone to cartilage interface. These magnitudes are shown in Figure 3.6.

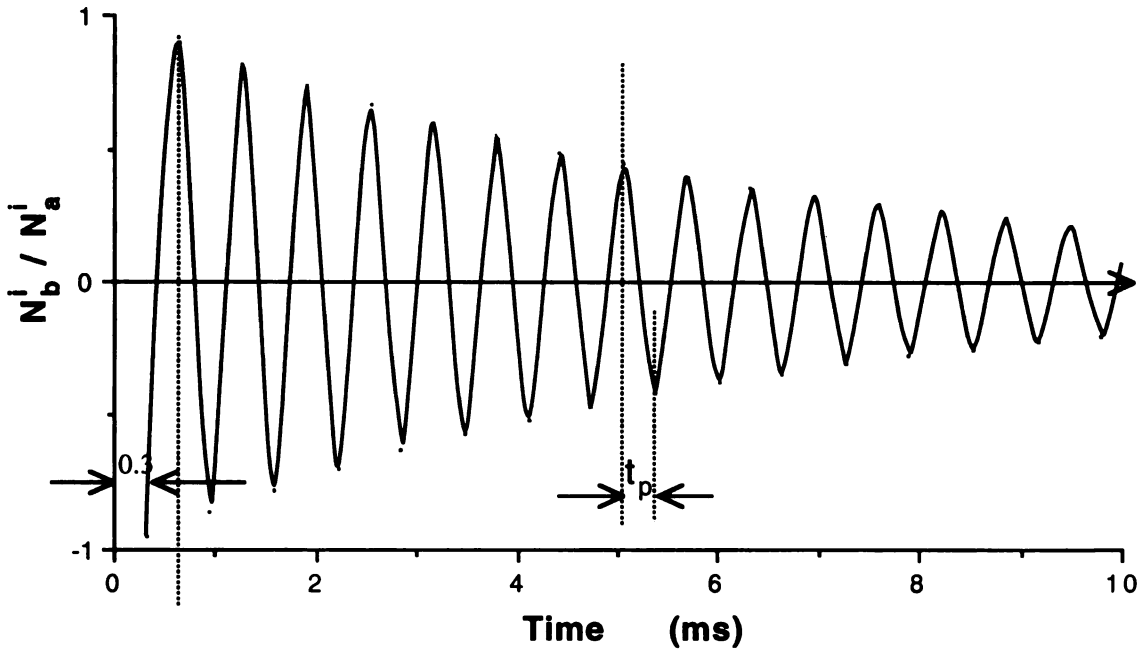

Figure 3.6 Reflected force at the cartilage-bone interface vs. time

The wave propagation velocity in the bone can be calculated using equation (3.13) and is equal to 33.33 mm/ms. If the thickness of bone is 10.0 mm, the time of wave propagation through the bone to the interface, t_p, can be simply calculated by dividing the bone thickness by wave velocity, c_1. Thus, t_p is equal to 0.3 ms/per half wave. Thus N_a^1 is equal to the value of the impact load at t=0.3 ms (Figure 3.7).

These curves of experimental impact load vs. time and reflected force at the bone-cartilage interface are shown in Figure 3.7. The magnitude of stress wave is 2 % of the peak impact load. Again, we have neglected damping of the material in this calculation, and our estimates are thus liberal.

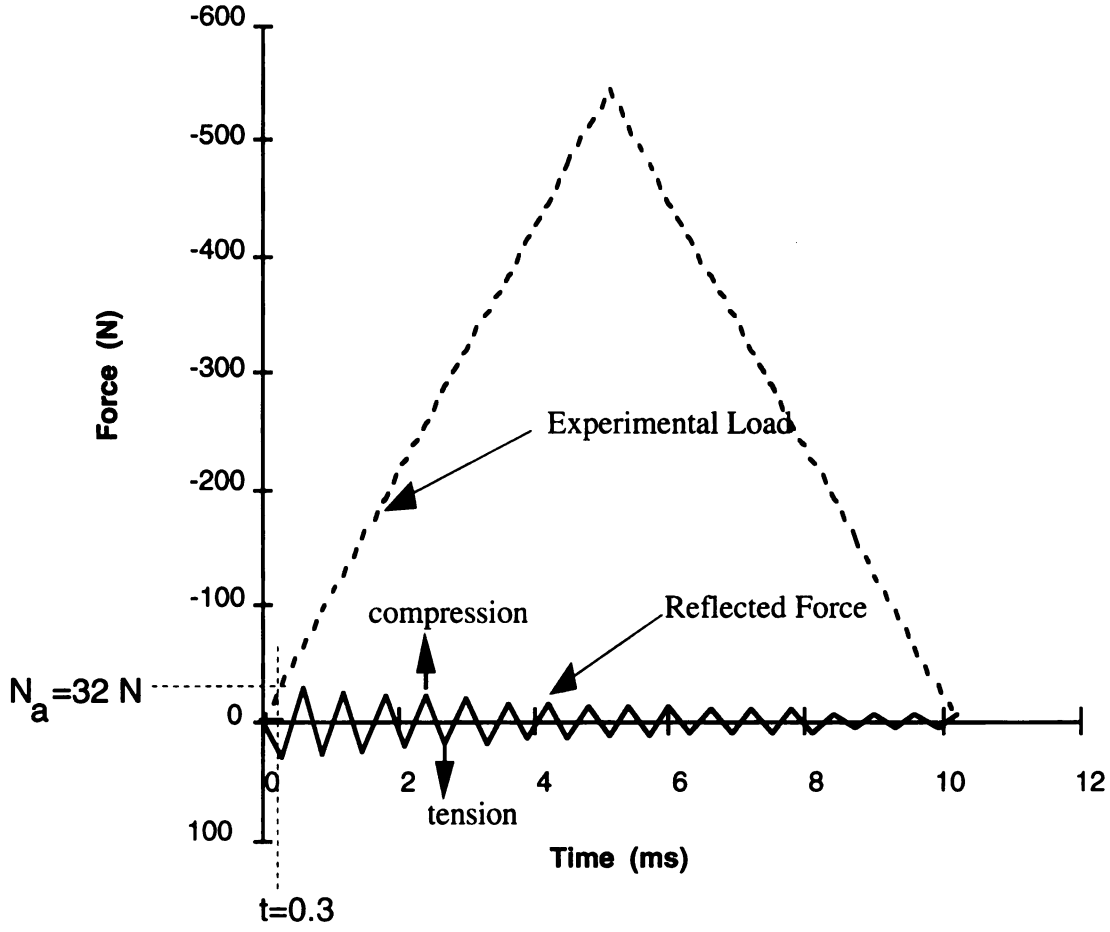

Figure 3.7 The effect of the reflected force on experimental impact load (bone to cartilage)

3.3 Plane Strain Modeling of the Rabbit Knee Joint and the Associated Boundary Conditions

The actual geometry of the animal knee joint and the loading locations are our focus in this study. For simplicity, a two-dimensional analysis was performed with plane strain conditions assumed in order to represent a confinement of the cross section.

The two-dimension plane strain model may be approximately taken place of the 3 dimension geometry, because of the character of the geometry character and the character of the fissures in the impacted cartilage (Figure 3.8 (b)). The size in the z direction of the

patella is larger than in the x and y directions, and the thickness of the patella cartilage is much smaller than the patella' s length in the z direction (Figure 3.11 (a)). The fissures are generally along with the z direction (Figure 3.8 (b)) so it seems that the stress field is independent of the z direction. Thus the actual geometry of the animal knee joint may be modeled by plane strain conditions. Figure 3.8 (a) shows our strain plane model assumption.

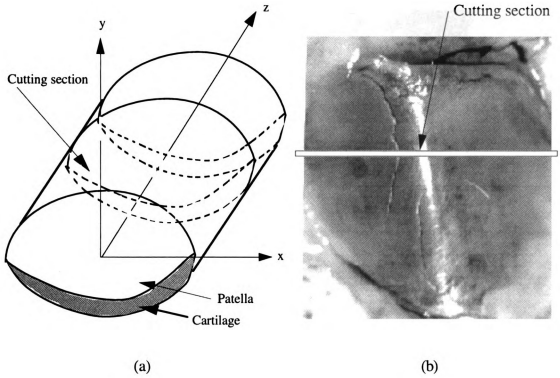

Figure 3.8 (a) Plane strain model of the patella. (b) Impact induced surface fissuring of cartilage

The boundary loads were obtained experimentally by recording pressures from Fuji film along a 0.5 mm thick zone at the cross section of interest on the anterior surface of the patella or PF contact pressures that were generated during blunt impact (Figure 3.9). The input loading profile on the anterior surface of the patella for the 2 Dimension model is plotted in Figure 3.10, and is used as the input loading condition of the FEM model.

The bottom of the femur of the rabbit knee joint is restrained in the x and y directions. A 2-D plane strain FEM model, the boundary conditions of the input load and the restraints are shown in Figure 3.11.

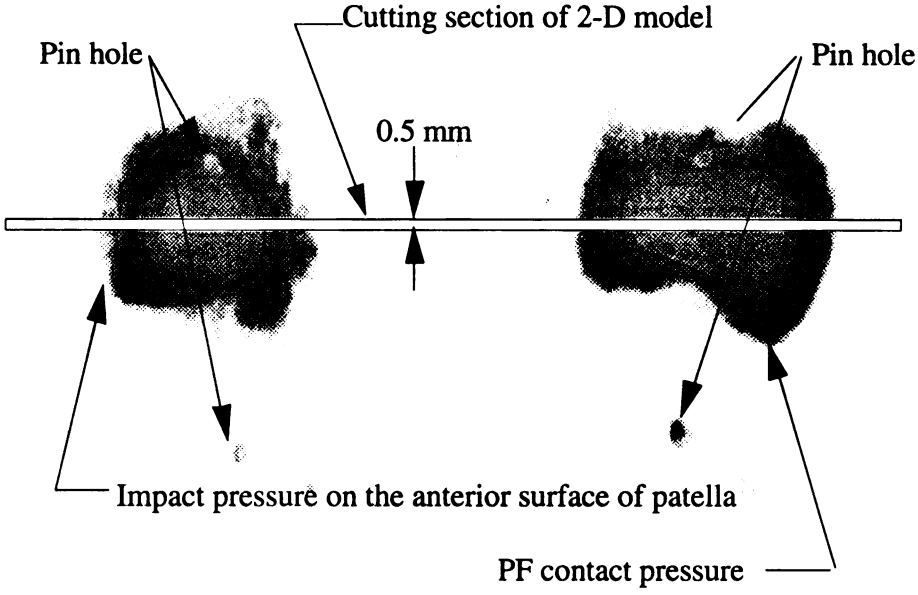

Figure 3.9 The contact pressure recorded with Fuji film on the anterior surface of the patella and the PF contact surface

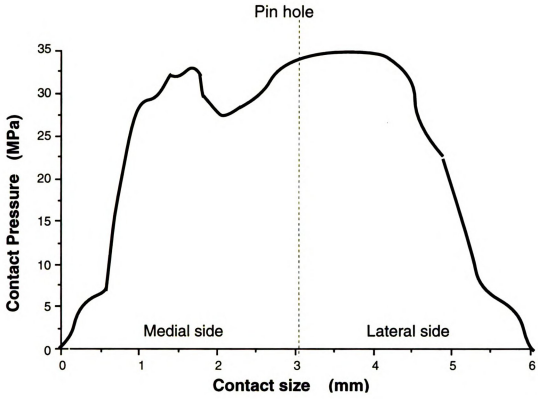

Figure 3.10 The profile of impact pressure on the anterior surface at the cut section

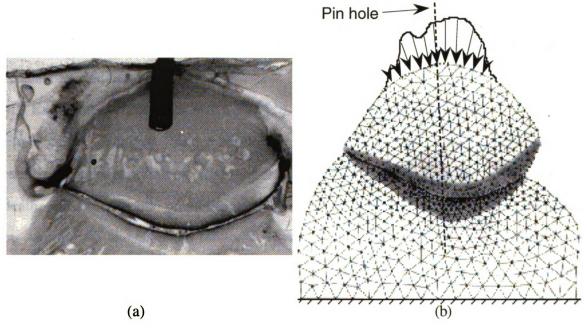

Figure 3.11 (a) The cross-section of the rabbit knee joint. (b) The 2-D FEM model and boundary conditions

Chapter 4 Estimation of the Unknown Material Properties of Cartilage Using an Inverse Approach

A primary aspect of this effort has been to develop a model of the joint to help explain injury mechanisms and to use in vivo results from the animal studies to predict in vivo human experiments. A problem that must be dealt with in any analytical model is material properties. Cartilage itself is a complicated biphasic material (Mow, et al, 1980), so the mechanical properties are difficult to define, especially for the analysis of blunt impact response. We justified (in Section 3.1) the use of an elastic model for situations in which impact load duration does not exceed 50 ms. This is indeed the case in a typical blunt impact to the knee (Haut, 1985). Eberhardt et al (Eberhardt, A. W., 1991), for example, uses mechanical properties obtained from indentation experiments and confined compression tests on cartilage performed by other investigators. However these data are documented for time duration longer than one second, which is much greater than the typical duration of a blunt impact.

4.1 Experimental Methods and a FEM Model of the Rabbit Knee Joint

Experimental data were collected from two mature (6-8 months of age) Flemish Giant rabbits. Impact experiments were performed on euthanized specimens within 1 hour of death. All experimental protocols were approved by the MSU All-University Committee on Animal Use and Care and followed NIH guidelines. Experiments were performed on the right (Experiment #1) and left (Experiment #2) limbs of one animal. The animal was held in position by insertion of a 3.2 mm diameter pin into the medullary canal via the greater trochanter (Haut, 1983). A bed of PMMA was placed at the proximal end of the femur to help distribute axial loads generated during knee impact (Figure 4.1). A 0.43 kg

mass was dropped onto the flexed limb from 0.2 meters.

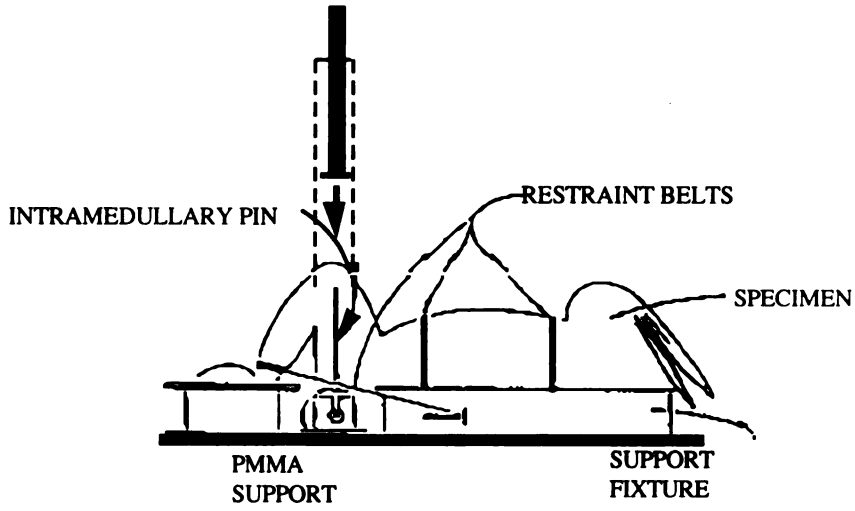

Figure 4.1 Schematic of the restraint system used for experiments #1 and #2. Note that the femur was constrained with an intramedullary pin inserted via the greater trochanter.

For a second animal (Experiment #3) the protocol followed that which has been used in previous in vivo studies (Haut, 1992). The animal was positioned supine with the right limb hyperflexed to align the femur vertically (Figure 4.2). The flexed limb was held in place against a rigid seat with spring-loaded clamps. The pelvis was also restrained with a strap to prevent rotation during blunt impact on the knee. A one-inch diameter, flat aluminum impact interface was attached to a load transducer and dropped on the patella from 0.46 meters. The total impact mass was 1.33 kg. This test protocol was known to produce surface fissures on patellar cartilage in a previous study (Haut, 1992).

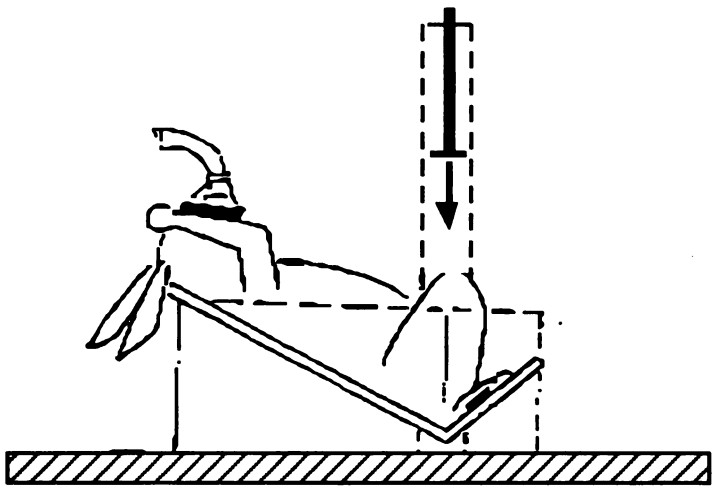

Figure 4.2 Schematic of the restraint system used in experiment #3. The hind limb was constrained with spring-loaded clamps and a strap across the pelvis

Impact force-time data were collected on a personal computer equipped with an analog-digital board sampling at 10,000 per second, A typical history of impact loading vs. time is shown in Figure 4.3.

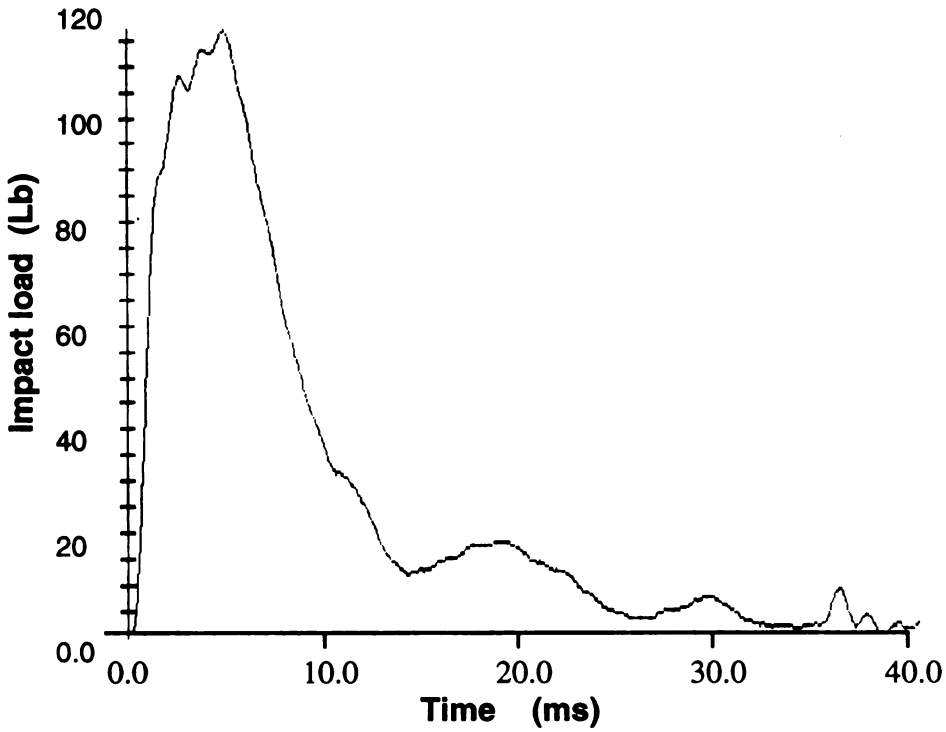

Figure 4.3 The curve of impact load vs. time in a typical experiment on rabbit knee joint

Two 1.0 mm diameter holes were drilled through the patella prior to blunt impact. Pressure sensitive film was inserted in the patello-femoral joint to record contact pressure distribution generated during blunt impact on the knee (Haut, 1989, Huberti, 1982). The film was encased in polyethylene and inserted under the patella and folded over the anterior surface of the patella. A hemostat was used to hold the film in place during impact, and no movement of the film was evident during impact. After each experiment, needle probes were inserted through each hole in the patella piercing the film and therefore locating the film with respect to the patella. The pressure sensitive film (Prescale, medium range, mono-layer, Fuji) was calibrated with a servo-hydraulic testing machine using a 100 ms haversine load pulse (Haut, 1989). The film was digitized with a video scanner and a personal computer-based analysis program (Image 1.44). The scanner sensitivity was 11.8 pixels per mm. The pressure data were documented across the entire contact area and also scanned medially to laterally across the patella at a cross section approximately midway between the two pin holes. This cross section was selected because it was the area which typically encompassed the largest contact pressures. This 2-D pressure profile served as the experimental data to compare with the theoretical results.

After the impact experiments, the hind limbs were removed intact by sectioning at the lumbar spine. The joint flexion angle was preserved while the limbs were immersed in a 10% formalin solution for approximately 3 weeks. After incubation, a single transverse cut was made with a diamond bladed saw through the patello-femoral joint at the location chosen for pressure analysis. Photographs of the joint geometry were enlarged and served as input to a finite element model (Figure 4.4 (a)). The surfaces of the cartilage on the patella were wiped with India ink and examined under a microscope at 25X for surface fissures.

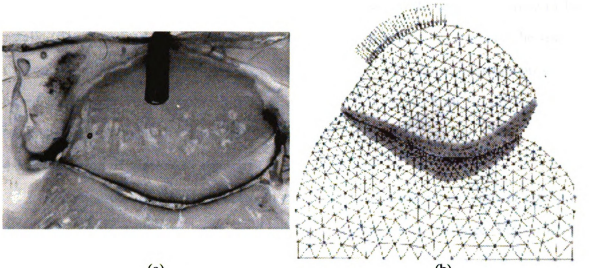

(a) (b)

Figure 4.4 (a) A section cut through the patello-femoral joint. (b) Typical FE mesh for 2-D analysis of the blunt impact response of the rabbit PF joint

A 2-dimensional finite element model of the joint was constructed using 1597 plane strain elements to model experiment 1, 1406 plane strain elements to model experiment 2 and 2577 plane strain elements to model experiment 3. The computer code employed was I-DEAS, Structural Dynamics Research Corporation, Milford, OH. . Assuming a frictionless contact surface, fifty to sixty gap elements 0.1 mm thick were used to simulate the joint space between the patella and the femur. The work followed that of Eberhardt et al (1990) in assuming that a linear elastic model was suitable for the analysis. The elastic modulus and Poisson's ratio of bone were assumed to be 2 GPa and 0.3, respectively (Cowin, S, 1987). The study involved correlation with the elastic modulus of cartilage varying from 1-20 MPa, and parameter analyses in which Poisson's ratio of cartilage was varied from 0.01 to 0.5. It was assumed that the bone and cartilage properties in the patella and femur were identical. This was based on an earlier study by Jurvelin, et al (1990) which found the "500 ms response" (shear modulus) of the canine femoral and patellar cartilage to be statistically identical. The boundary loads were obtained experimentally by recording pressures on a 0.5 mm thick zone at the cross

section of interest that were generated during blunt impact in the anterior surface of the patella (See Chapter 3.4). A mathematical routine was developed to compute the sum of the squared differences (residuals) between the computed and measured contact pressures, based on data at 50 locations in a single slice of the patello-femoral surface. This parameter helped quantify the material properties of the cartilage.

4.2 Estimation of Material Properties

The degree of correlation between experimental and theoretical contact pressures in the PF joint depended on the material properties chosen for the cartilage (Figure 4.5 a). As the value of Poisson's ratio approached 0.5 for the cartilage, the residuals decreased (Figure 4.5 b). We also noted that the residuals were a minimum for an elastic modulus of approximately 2 MPa for the cartilage at Poisson's ratio 0.49 (Figure 4.5 a). The residuals were significantly higher for all values of elastic modulus when Poisson's ratio of the cartilage was chosen to be less than approximately 0.49, for example (Figure 4.5b). The degree of correlation did not change as the modulus of bone was altered from 1 GPa to 20 GPa.

The calculated results of Experiment #3, by the method of minimization residuals, are shown in Figure 4.5 and 4.6. The same processes were used for Experiment #1 and #2. The minimum residual of PF contact pressure between the FEM model and the experiment occurred at a Young's modulus equal to 2 MPa and Poisson's ratio equal to 0.49. The details of these analysis are presented in a recent paper (Li, X., et al, 1994).

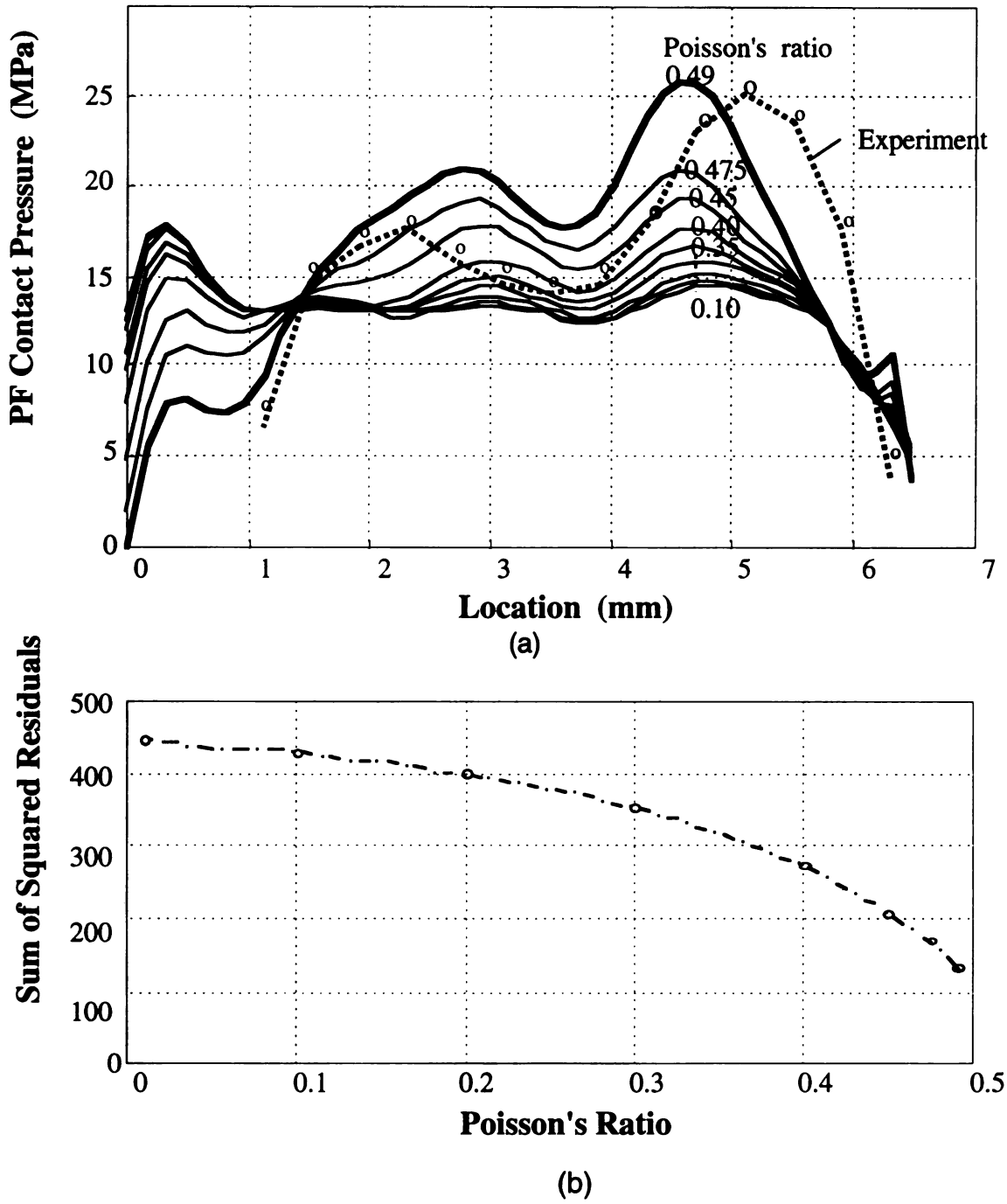

Figure 4.5 (a) A plot showing the experimental contact pressure distribution and the corresponding theoretical distributions for various values of Poisson's ratio at Young's modulus 2 MPa. Note how well the results at 0.49 compare to the results from experiments #3, (b) The residuals decreased continuously as Poisson's ratio approached 0.49

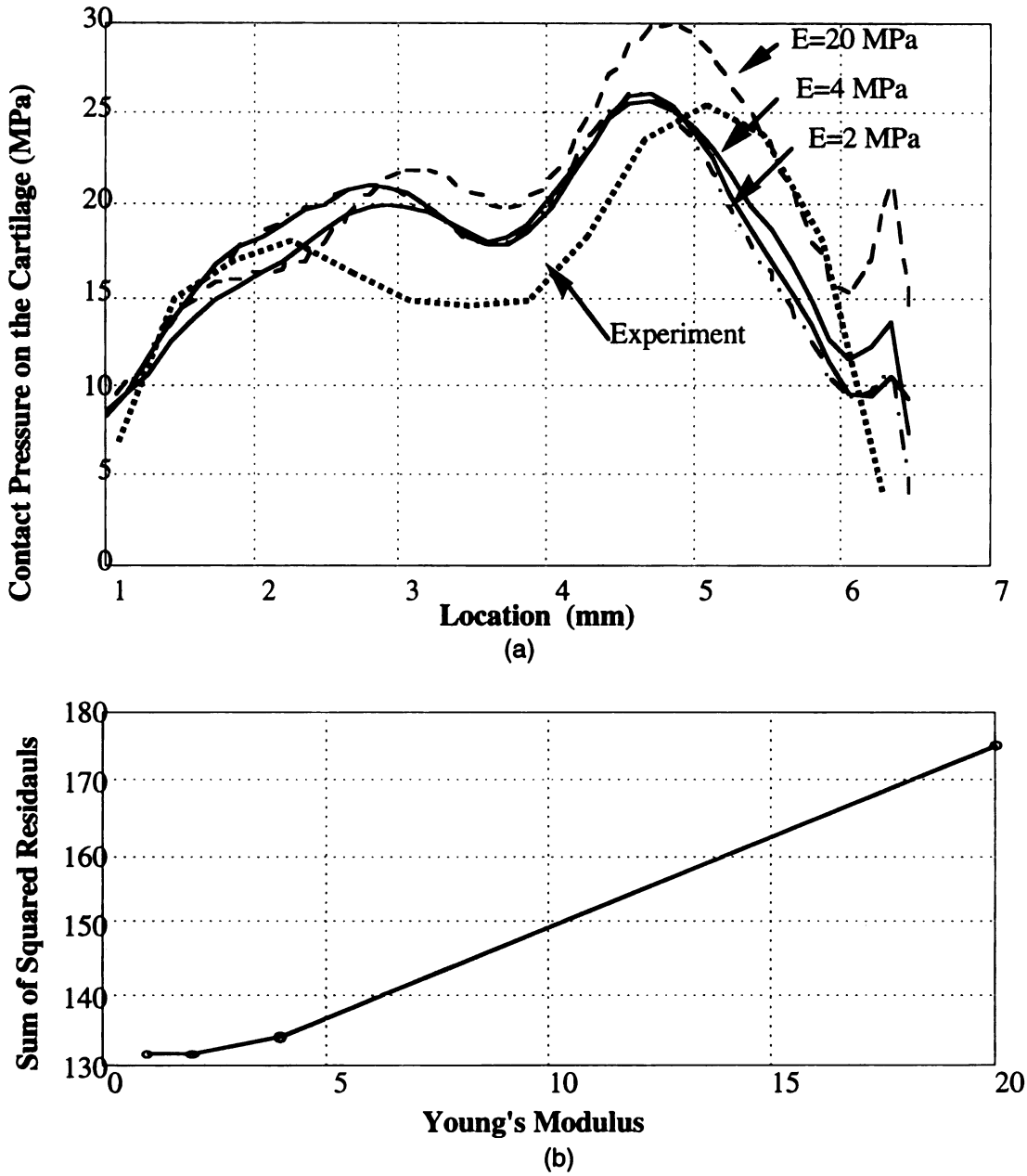

Figure 4.6 (a) The effect of variations in the elastic modulus of cartilage on the residuals computed between the experimental and the theoretical contact pressures. A minimum was obtained for an elastic modulus near 2 MPa for the cartilage at Poisson's ratio of 0.49, (b) The residuals reached minimum at a Young's modulus of 1 to 2 MPa at a Poisson's ratio of 0.49

The primary objective of this study was to develop an analytical model of the rabbit's patello-femoral joint that could be used to study the stresses and strains generated

during a blunt impact. The differences between the model generated contact pressures and experiment were minimized when Poisson's ratio was 0.49 for the layer of cartilage. This result was consistent with the biphasic model of Mow (1980), and agreed with Eberhardt et al (1990) and Askew and Mow (1978) who selected values of 0.475 and 0.45, respectively, in their elastic models. In our study the difference between theory and experiment was also minimized when an elastic tensile modulus of 2 MPa was chosen for the layer of cartilage. In the joint model of Askew and Mow (1980), a value of 12 MPa was chosen for the analysis. Eberhardt et al (1990) chose a value of 1.5 MPa for the elastic shear modulus of the cartilage (which corresponds to a tensile modulus of approximately 4.4 MPa if one assumes isotropy of the layer). Our laboratory is also studying the mechanical properties of patellar cartilage using an indentation relaxation experiment (Haut, 1992). The analysis follows that presented by Hayes et al (1972) and is based on the elastic solution of a layer bonded to a rigid half-space. The patellar cartilage is indented 0.1 mm using a rigid probe. An instant shear modulus of the layer is evaluated from the analysis approximately 50 ms after its deformation. The experiment includes a period of relaxation in which the rate of load relaxation and the equilibrium responses are documented (Haut, 1992). The instant shear modulus of the rabbit's patellar cartilage determined by this technique was approximately 0.46 +/- 0.17 MPa. The optimum value of tensile modulus from the current study (i.e. 2 MPa) corresponds to an elastic shear modulus of approximately 0.67 MPa. We see, therefore, that there is good agreement between the elastic shear modulus determined via the whole joint model and the results obtained in the short-time indentation experiment using an elastic analysis.

Chapter 5 Application of the FEM Model and Probability Analysis of Damage Prediction

In order to study the mechanisms of cartilage damage in Ide's experiments, I have used the previously discussed FEM model and examined the distribution of stress and strain in an attempt to correlate these parameters with injury. This correlation has used a logistic regression analysis correlating various mechanical parameters with the incidence of the surface fissures. In Ide's experiments, contact loads on the anterior surface of the patella were not recorded. Therefore, the FEM model used to analyze Ide's experiments had to be changed. In order to study the distribution of stress and strain in the patella, I used the measured contact pressures in the patello-femoral joint as the input for loading boundary conditions (Figure 5.1). The analysis was performed using the geometry and assumptions discussed in Section 3.4.

5.1 FEM Analysis of the Rabbit Knee Joint Impact Tests

FEM Model and Boundary Conditions

The geometry for the 2-dimensional finite element model was copied from an actual section of a typical patella. This FEM model was constructed using 800 plane strain elements (Figure 5.1). The Young's modulus and Poisson's ratio for bone were assumed to be 2 GPa and 0.3, respectively (Cowin, 1987). The Young's modulus and Poisson's ratio for cartilage were assumed to be 2.0 MPa and 0.49, respectively. The values were obtained by the inverse method discussed in the Chapter 4.

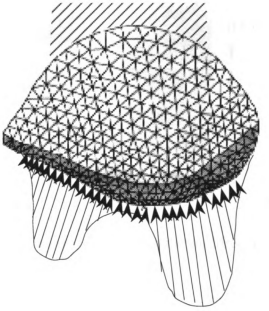

5.1 Typical FE mesh for the 2-D analysis of the blunt impact response of the rabbit patella for Ide's experiments (1992)

The measured contact pressures shown in Figure 5.2 (Ide, 1992) were used as the input boundary conditions at the cartilage surface (Figure 5.1). The contact pressure distribution was documented across the lateral and medial facets of the patella by taking a 0.5 mm thick slice of the distribution and generating a 2-dimensional pressure profile (Figure 5.3). The anterior aspect of the patella was rigidly fixed (Figure 5.1). From Ide's experimental data, thirty-four different input loads were used in the FEM model to obtain the related stress fields.

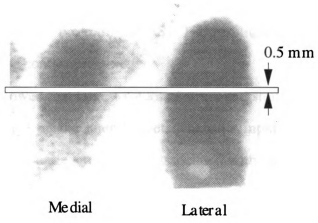

Figure 5.2 Contact pressures recorded by Fuji film during Ide's experiments

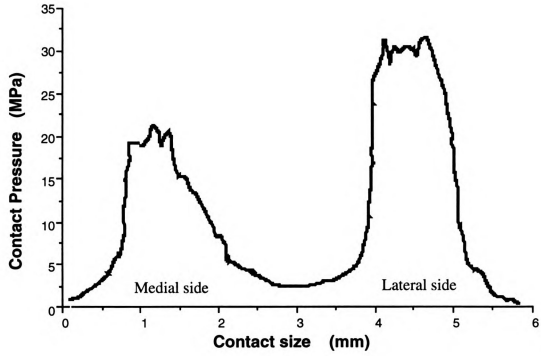

Figure 5.3 A 2-D profile of these PF contact pressures.

Analytical Results

Ide's experiments described in Section 2.1 indicated that the incidence of surface fissures correlated well with the occurrence of a bimodal distribution of contact pressures

on the patellar facets. The contact pressures distributions were input into the patella FEM model which employed the program IDEAS. The resultant distributions of stress and strain varied with these contact pressures.

The results showed that largest values of stress and strain occurred near the center of the patellar cartilage on the lateral facet, when the input loading was a biomodal distribution. The area of large stresses was associated with the area where Ide observed surface fissures after blunt impact (Figure 5.4). Typical contour plots of the stress and strain in the cartilage layer are shown in Figures 5.5 (a), (b), (c) and (d). The maximum values of each parameter along the surface of the lateral facet are also given in Table 5.1.

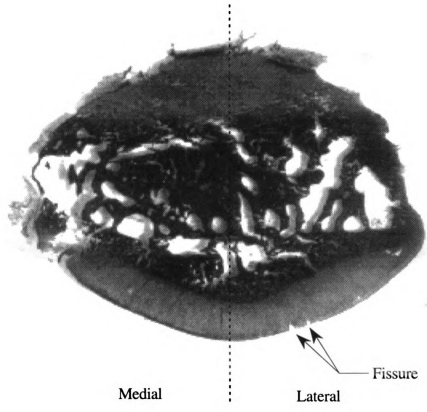

Figure 5.4 A typical location of surface fissuring measured often a severe blunt insult.

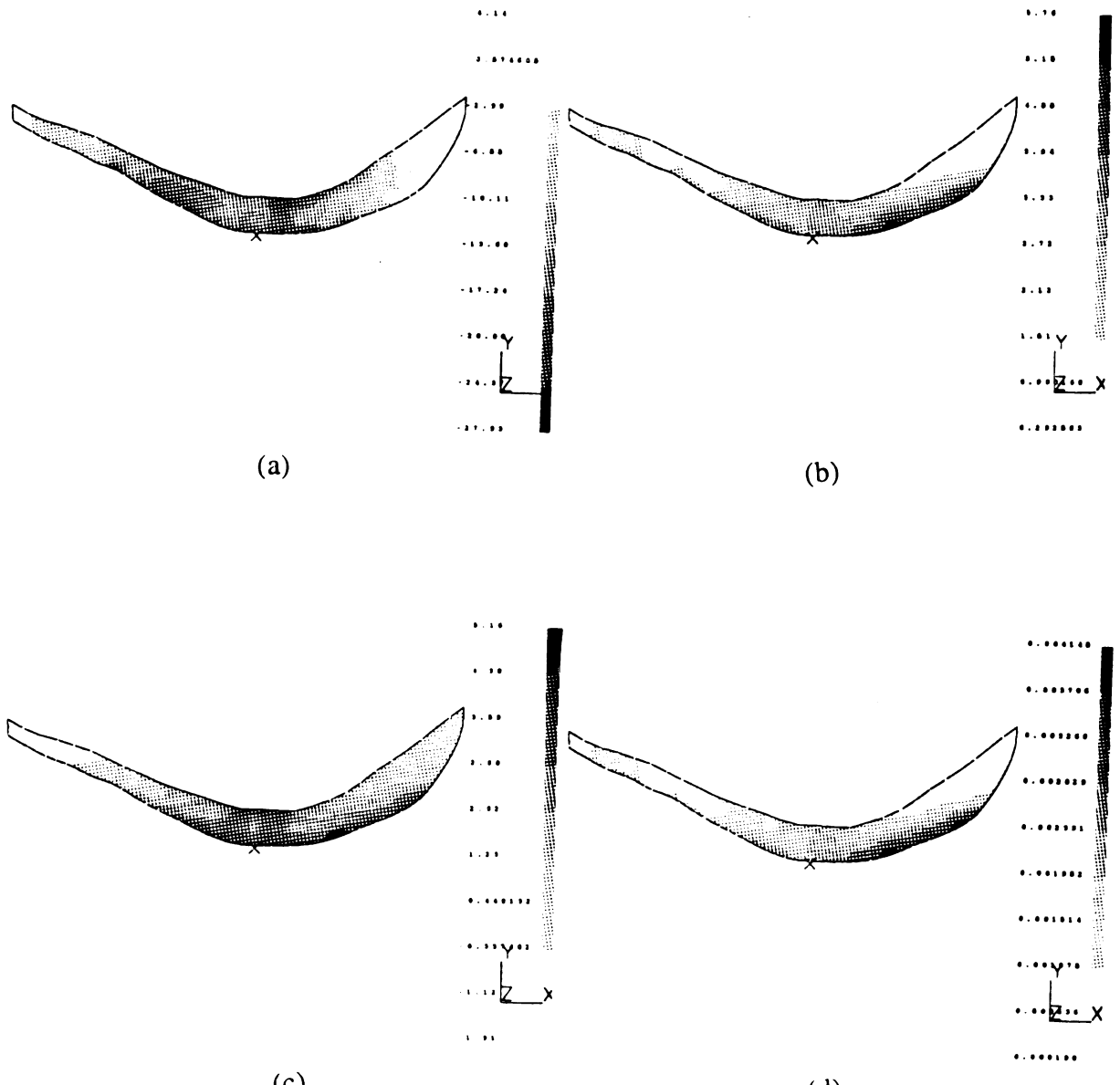

Figure 5.5 Typical contour plots for the stress and strain distributions in cartilage, (a) the minimum principal stress distribution, (b) the maximum shear stress distribution, (c) the shear stress distribution, τ_{xy}, and (d) the maximum tensile strain distribution

The results show that a few maximum values for maximum shear stress, tensile strain and mean stress appear near the damage zone. In order to correlate each mechanical parameters with the cartilage damage, the maximum values of each variable along the lateral patellar surface are listed in Table 5.1, and plotted in Figure 5.6 (a), (b), (c), and (d). These data were analyzed using a logistic regression statistical model to determine the best predicted articular cartilage damage.

The data shown in Figure 5.6 indicate that there is a correlation between the magnitudes of contact pressure, maximum shear stress, maximum strain, peak contact pressure and the occurrence of surface fissures. In order to quantify the predictive power of each parameter, a logistic regression analysis was conducted in the next section.

Table 5.1 Analytical results from the FEM model based on Ide's experimental data

Fissure	Strain %	Mean stress (MPa)	Max. Shear stress (MPa)	C0.05 (MPa)	C0.1 (MPa)	C0.2 (MPa)	C0..3 (MPa)	C0.4 (MPa)	C0.5 (MPa)
*1	0.115	30.14	3.69	5.19	6.7	9.71	12.7	15.74	18.76
2	0.115	17.25	1.9	2.76	3.62	5.35	7.07	8.8	10.52
1	0.13	23.65	2.25	3.43	4.61	6.98	9.34	11.71	14.07
2	0.179	21.79	2.78	3.86	4.95	7.13	9.31	11.49	13.67
1	0.271	34.47	3.62	5.34	7.07	10.5	14	17.41	20.86
1	0.261	31.78	4.14	5.73	7.32	10.5	13.7	16.85	20.03
1	0.232	23.87	3.6	4.79	5.99	8.37	10.8	13.15	15.54
2	0.213	30.19	3.45	4.96	6.47	9.49	12.5	15.53	18.55
2	0.172	19.72	2.7	3.69	4.68	6.65	8.62	10.59	12.57
1	0.234	25.2	3.22	4.48	5.74	8.26	10.8	13.3	15.82
1	0.22	27.15	3.56	4.91	6.27	8.99	11.7	14.42	17.13
1	0.24	30.85	3.82	5.36	6.9	9.99	13.1	16.16	19.24
2	0.266	29.05	3.53	4.98	6.43	9.34	12.2	15.15	18.05
2	0.234	20.87	3.55	4.59	5.63	7.72	9.81	11.89	13.98
2	0.054	8.59	0.9	1.33	1.76	2.62	3.48	4.34	5.2
2	0.21	21.76	3.26	4.35	5.44	7.61	9.79	11.97	14.14
2	0.257	29.79	4.05	5.54	7.03	10	13	15.96	18.94
2	0.15	18.57	2.54	3.47	4.4	6.26	8.11	9.97	11.83
2	0.208	22.31	3.25	4.36	5.48	7.71	9.94	12.17	14.4
2	0.205	23.78	3.21	4.4	5.58	7.96	10.3	12.72	15.1
2	0.112	17.21	1.86	2.72	3.58	5.3	7.02	8.74	10.46
1	0.217	27.24	3.45	4.82	6.18	8.9	11.6	14.35	17.07
1	0.17	28.93	2.83	4.27	5.72	8.61	11.5	14.4	17.29
2	0.059	9.71	0.99	1.47	1.96	2.93	3.9	4.87	5.84
2	0.136	15.3	2.11	2.88	3.64	5.17	6.7	8.23	9.76
1	0.196	30.65	3.22	4.75	6.29	9.35	12.4	15.48	18.55
1	0.292	33.81	4.6	6.29	7.98	11.4	14.8	18.13	21.51
1	0.279	30.99	4.38	5.93	7.48	10.6	13.7	16.77	19.87
1	0.262	26.34	4.04	5.36	6.68	9.31	12	14.58	17.21
1	0.361	32.33	5.51	7.12	8.74	12	15.2	18.44	21.67
1	0.282	25.13	4.29	5.55	6.8	9.32	11.8	14.34	16.86
2	0.177	21.02	2.8	3.85	4.9	7	9.1	11.21	13.31
2	0.172	22.21	2.71	3.82	4.93	7.15	9.37	11.6	13.82
1	0.226	21.64	3.476	4.56	5.64	7.8	9.97	12.13	14.3

*, "1" means the specimen fissured and "2" means no surface fissures were recorded. In Table 5.1, c0.05, c0.1, c0.2, c0.3, c0.4 or c0.5 is a combination stress of shear stress with 5%, 10%, 20%, 30%, 40% or 50% mean stress.

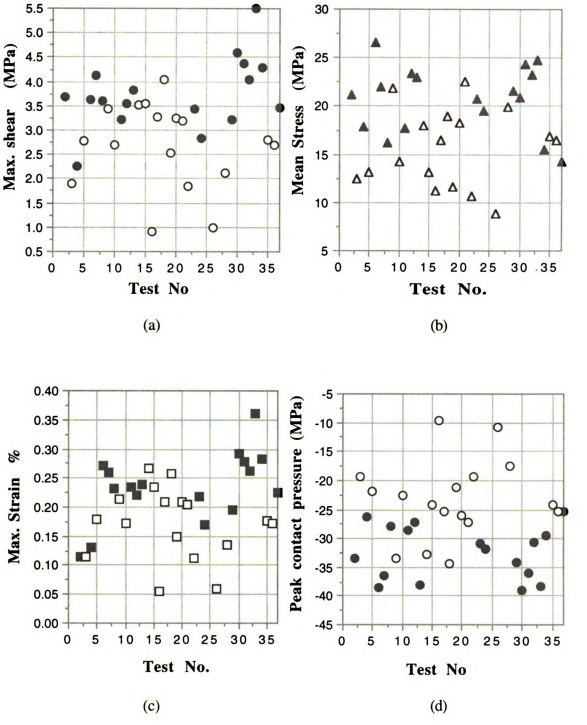

Figure 5.6 A correlation between the maximum values of each indicated parameter and the occurrence of surface fissures on the cartilage. (a) maximum shear stress, (b) mean stress, (c) maximum strain, and (d) peak contact pressure.

5.2 Probability Analysis

A logistic regression program (Crunch 4) was used to perform the analysis. The data in Table 5.1 was used as the data base to find out the best predictor of surface damage. The results of this analysis are presented in Table 5.2 and plotted in Figure 5.7. The occurrence of a surface fissure on the lateral patella facet in Ide's experiments correlated best with the magnitude of contact pressure (82.1%). Maximum shear and maximum strain were not as good of predictors; being 76.5%. The analysis also allows an analysis of combining various effects. Keeping in mind the discussion given in Section 2.3 for the use of a Coulomb-Mohr type of criterion, the values of this combination of shear stress and the part of mean stress for each experiment are also shown in Table 5.1. The logistic regression analysis indicated that the best predictor of surface fissuring was 85.3% , when c was equal to 0.1. The predictability of this combination stress exceeded that simply using contact pressure, per se. (Figure 5.7 and Table 5.2)

These general results indicate that a Coulomb-Mohr type of the failure criterion is reasonable for predicting cartilage damage. In the following sections, an experimental approach will be presented to independently determine the value of c.

Table 5.2 Logistic regression results

Variable	S.E	p Value	Optimal point	Overall Probability %
Max. Strain	7.49	0.0149	0.445	76.5
Mean Stress	0.114	0.0026	0.587	82.4
Max. Shear	0.76	0.0085	0.356	76.5
C 0.05	0.67	0.0063	0.524	79.4
C 0.1	0.55	0.0051	0.559	85.3
C 0.2	0.39	0.0039	0.51	82.4
C 0.4	0.23	0.0034	0.507	82.4
Average Pressure (Ide)	0.11	0.0027	0.587	82.4

Note, in Table 5.2, S.E is the estimated standard error; p value is associated with the chi-square; the optimal point is the cutpoint to obtain the derived dichotomous variable, and the last column given the overall probability.

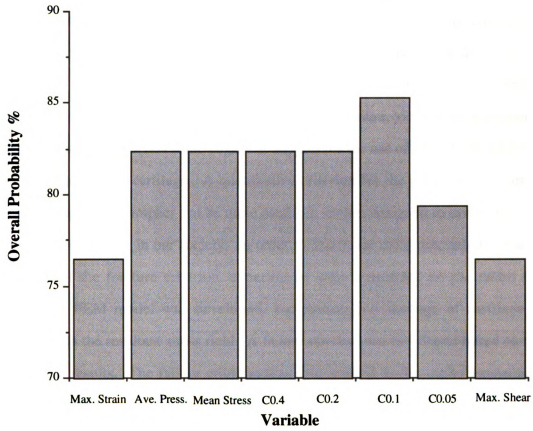

Figure 5.7 The comparison of the prediction power of each variable given in Table 5.2

Chapter 6 Determination and Application of a Coulomb-Mohr Failure Criterion

The probability analysis given in Chapter 5 was conducted for those factors that may produce damage of cartilage. The probability analysis was an important factor in generating a qualitative explanation of tissue damage. The results showed that the interaction of two variables, shear stress and hydraulic pressure, yielded the best predictor of tissue damage. This lends some degree of support for the use of a Coulomb-Mohr type of failure criterion for cartilage. A quantitative criterion for the prediction of cartilage damage during a blunt impact can be quite useful in studies designed to investigate ways of mitigating the injury in our society. In order to determine more precisely the material parameters of the fracture criterion, experiments were conducted on the rabbit tibial plateau. An FEM model was developed, and histological damage of cartilage was correlated with the resultant stress field. A failure envelop was developed based on these experimental results. The failure criterion was then applied to the earlier experimental data of Ide (1992).

6.1 Impact Tests on the Rabbit Tibial Plateau

The Experimental Method

The objective of the earlier impact tests on rabbit knee joints (Haut and Ide, 1992) was to study the impact parameters useful in predicting surface fissures on cartilage, document fissure location, and correlate contact pressures with cartilage damage. It is hard to use these data directly to determine the reason of initial damage of cartilage and bone, because tissues damages may be affected by many experimental factors; such as loading location, rate of loading and the geometry of each specimen. In order to determine the critical parameters of cartilage damage, I chose a simplified geometry to help with repeatability of experimental conditions and generate a more controlled loading

condition. The rabbit tibial plateau was selected for these experiments, because the surface is flat and smooth, and its thickness is nearly constant. Tibia plateaus from 20 Flemish Giant rabbits (6-8 months of age) were used for the impact experiments. The animals were being used in other studies. The tibia plateau was fixed in a plastic tube with PMMA (Figure 6.1), and covered with a saline moistened cloth prior to each experiment. The quality of the cartilage surface was checked before each test to make sure there were no pre-existing fissures or other pathologies on the cartilage surface. Experimental data were collected from impact experiments within 1 hour of death.

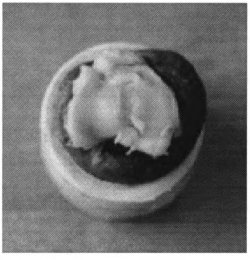

Figure 6.1 Surface view of the rabbit's tibial plateau.

In order to document initial damage of cartilage on the tibial plateau, an impact device was developed. The device had an adjustable grip which could be adjusted to orient the surfaces so they would be perpendicular to the indenters (Figure 6.2). A sensitive load cell (50 Pound) was mounted on the indenter. The indenter head was spherical with radii of 2.0, 4.0 or 20.0 mm. The indenter masses were 27.4, 28.6 and 30.0 grams, respectively.

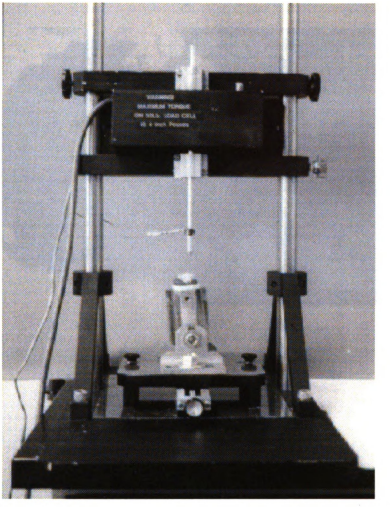

Figure 6.2 The impact device

In order to locate the contact area during impact, India ink was painted on the indenter before each experiment. The contact area was marked clearly, and some of the ink penetrated the surface, depending on the extent of surface damage. This helped document surface fissures using a microscope. A typical example of surface fissuring is shown in Figure 6.3.

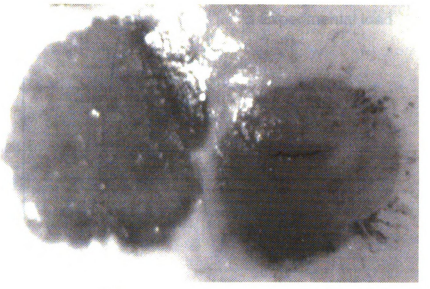

(a) (b)

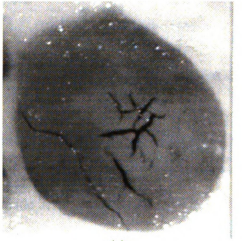

(c)

Figure 6.3 Surfaces fissures located in the contact area after impacts. These are enhanced with India ink. The diameter of this mark was approximately 2.0 mm. (a) before initial fissuring, (b) initial fissuring and (c) fissures after severe impact

The impact force-time data were collected on a personal computer equipment with an analog-digital board sampling at 10,000 per second. The typical loading time was less than 1.0 ms. A typical plot of load vs. time is shown in Figure 6.4.

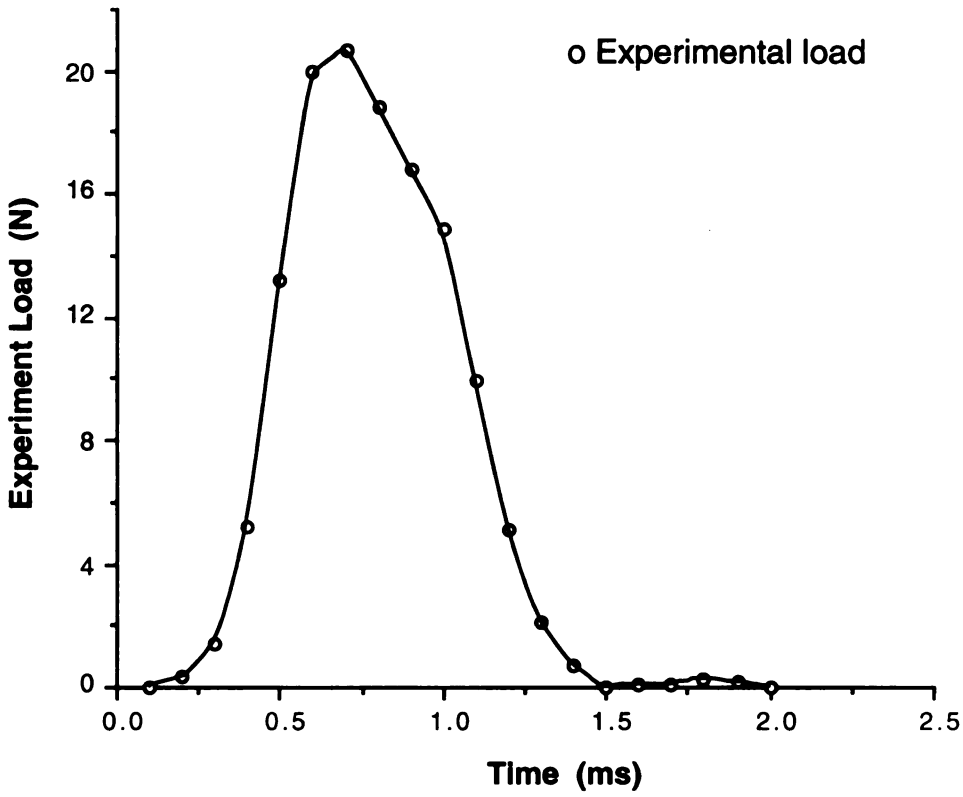

Figure 6.4 Load vs. time recorded with a 2.0 mm radius spherical indenter impact test

The contact surface was examined with a microscope at 50 power after each impact (Figure 6.3). Histological slides were prepared using standard methods. The histological sections were made across each impact location. These sections were cut at 6 micron, stained with safranin o -fast (green) and examined at 400 power. A histological technician (J.W.) also examined each section to rule out preparation artifacts.

Results of the Indentation Experiments

Impact tests were conducted using different three impact indenters. The first group, for which a 2.0 mm radius indenter was used, consisted of seventy-six experiments. Thirty-four of the specimens suffered obvious damage on the cartilage surface. When an impact load reached 30 N, there was a 84.3 % probability of generating a fissure on the cartilage. The peak load, the drop height and the resultant cartilage

damage for this group of experiments is shown in Figure 6.5. The critical load (30 N) which resulted in cartilage fissuring was used as input for FEM model discussed in next Section. In the second group a 4.0 mm radius impact indenter was used in fourteen experiments. Seven of these specimens had surface damage. When the impact load reached 45 N, there was a 87.5 % probability of observing a fissure. The results of experiments are shown in Figure 6.6. In the third group, a spherical indenter of 20.0 mm radius was dropped onto 16 specimens. In this case when the impact load reached 50 N, there was an 85.7 % probability of observing damage to the surface of the cartilage. Seven samples showed damaged. The results of impact experiments are shown in Figure 6.7.

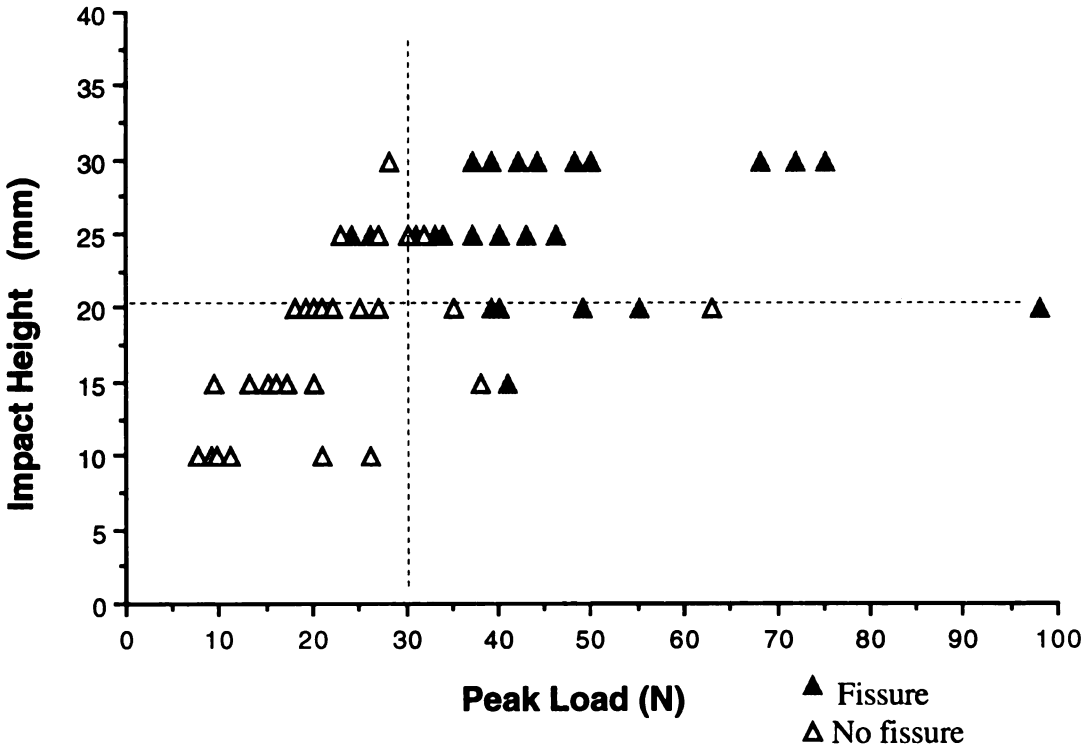

Figure 6.5 The experimental results from impact tests in group 1

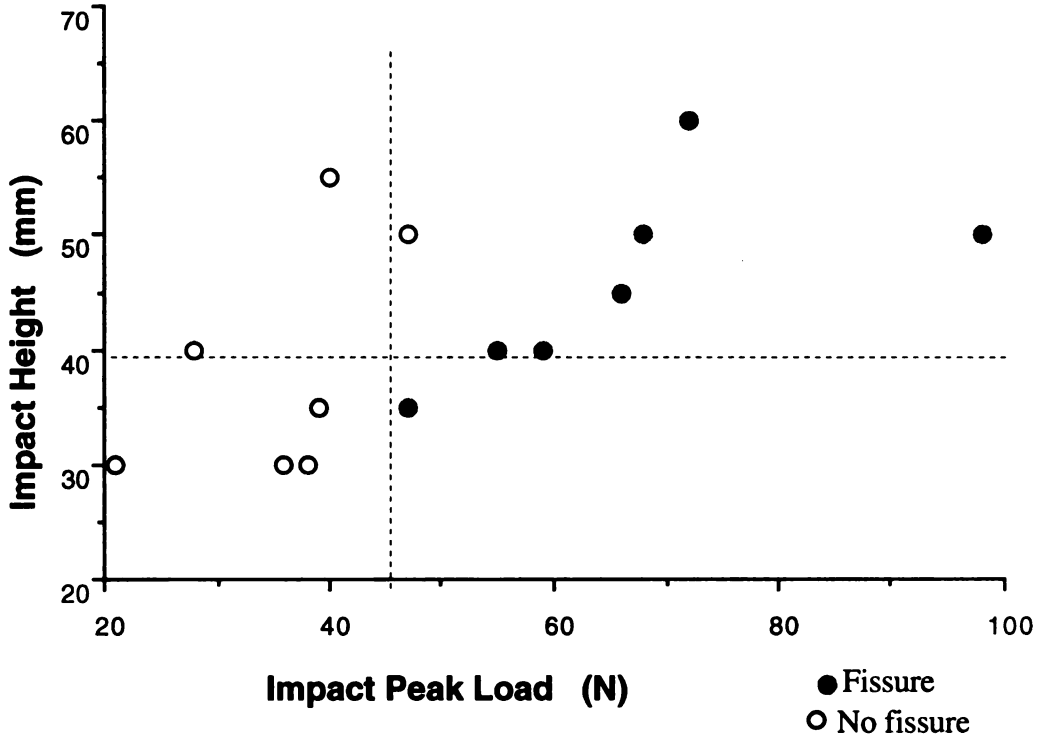

Figure 6.6 The experimental results from impact tests in group 2

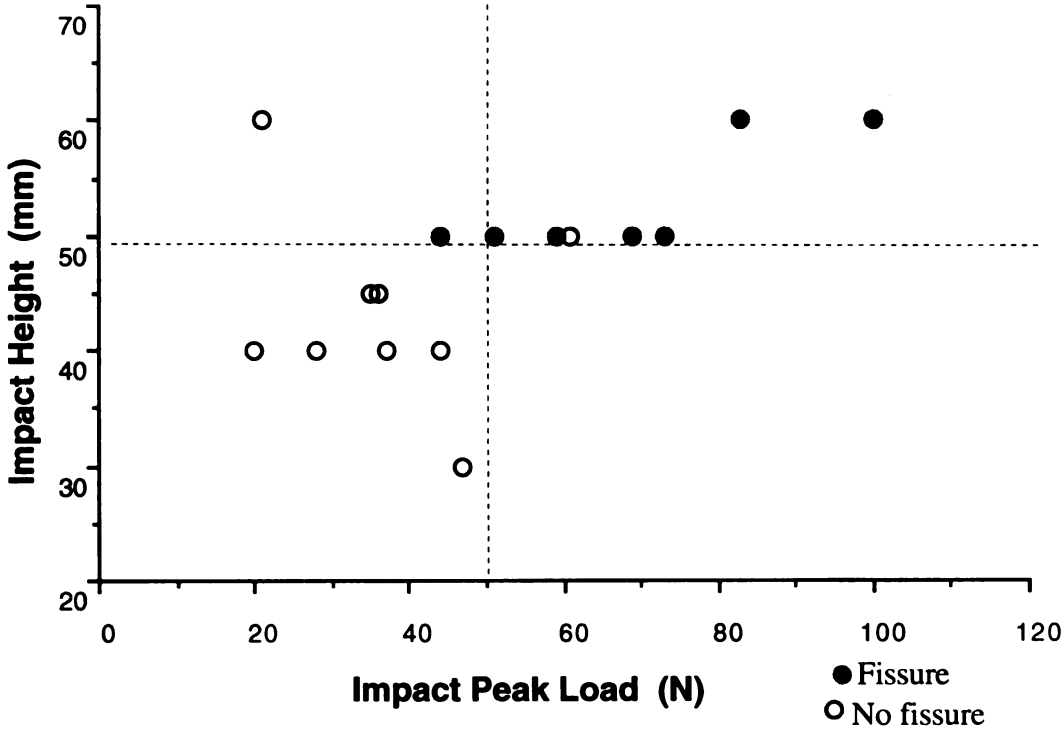

Figure 6.7 The experimental results from impact tests in group 3

Histological Observations

The damaged specimens from test in group 1 only showed surface injuries at the center of the contact zone. The fissures (splits) were oriented approximately either 40 or 90^{o} to the cartilage surface(Figure 6.8) . No residual deformations were observed at 400 power.

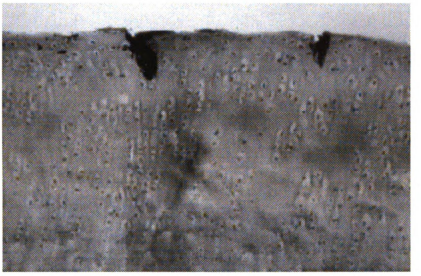

Figure 6.8 Typical fissures from specimen in group 1

In tests in group 2, the initial damage in six specimens occurred on the cartilage surface. The fissures were oriented approximately either 40 or 90^{o} to the cartilage surface, and most fissures were located in the center of the contact zone (See Figure 6.9). Damage was recorded in one specimen deeper in the zone of calcified cartilage. This fissure (or crack) occurred along the tide mark and above the subchondral bone (Figure 6.10).

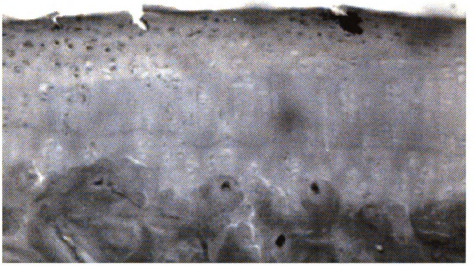

Figure 6.9 Typical fissures from specimen in group 2

Figure 6.10 A deeper microcrack generated in the specimen of group 2

In tests of group 3, 4 out of 7 specimens suffered surface damage. These fissures again had an angle of approximately either 40^{o} or 90^{o} to the cartilage surface and most fissures were located in the center of the contact zone (Figure 6.11). In three specimens damage was recorded in the calcified cartilage below the tide mark (Figure 6.12).

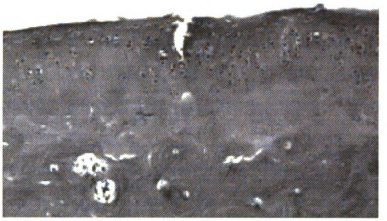

Figure 6.11 A typical surface fissure from specimen of group 3

Figure 6.12 Microcracks generated in a test specimen from group 3. Note the India ink on the cartilage surface

6.2 A FEM Model of Impact on the Rabbit Tibial Plateau

In this Section, a quasi-static, elastic, finite deformation, axisymmetric FEM model of the tibial plateau was developed using ABAQUS (Figure 6.13). Model analysis was performed for three different indenters of radii 2.0, 4.0 and 20.0 mm. These

aluminum indenters are assumed to be rigid, smooth spheres. For simplicity of geometry, a constant thickness of the cartilage layer was assumed. This thickness was assumed to be 0.5 mm, which is an average value recorded on one tibial plateau. The thickness of bone was assumed to be 1.5 mm, which is an average value measured from the PMMA base to the top of the plateau in one experiment. A total of 165 axisymmetric elements were used in this model. Fifteen of these were frictionless interface elements between the indenter and the cartilage surface.

Young's modulus and Poisson's ratio for the cartilage were assumed to be 2 MPa and 0.49, based on the rabbit patella study using the results discussed in Chapter 4. The Young's modulus and Poisson's ratio of bone were assumed to be 2 GPa and 0.3, respectively (Cowin, 1987).

The tibial bone was restrained in the x and y directions, and a quasi-static load was applied to the cartilage surface by a half sphere (Figure 6.14). This quasi-static load was approximately equal to the measured impact loads (Figure 6.4) which caused initial damage of cartilage in the tests discussed in the Section 6.1. The input load history was linear related to time. At time 1 ms, the input peak loads in the FEM model were 30 N, 45N, and 50 N for the 2.0, 4.0 and 20.0 mm radius indenters, respectively.

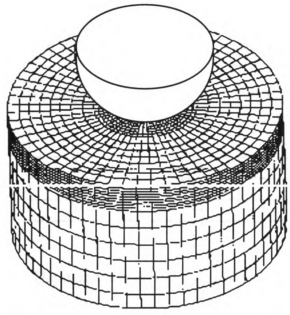

Figure 6.13 3-D tibia impact model

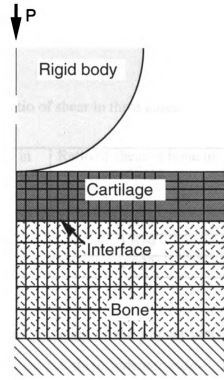

Figure 6.14 Axisymmetric model

Analytical Results

In all three loading cases, the maximum compressive principal stress occurred in the center of the contact area (Figure 6.15). They were 8.4, 11.4 and 21.4 MPa for the cases of the 2.0, 4.0 and 20.0 mm radius indenters, respectively.

The highest maximum shear stresses occurred in two areas: at the center of the contact zone and in the bone just below the cartilage-bone interface (Figure 6.16). The magnitudes of maximum shear stress at the center of the contact area in the 2.0, 4.0 and 20.0 mm indenter cases were are 2.82, 3.16 and 3.71 MPa, respectively. The direction associated with the maximum shear stresses was in the range of 35^{o} to 45^{o} (Figure 6.16). The maximum shear stresses in the bone for the 2.0, 4.0 and 20.0 mm indenter cases were approximately 4.08, 5.35 and 7.54 MPa, respectively. The directions of these maximum shear stresses were in the range of 20^{o} to 45^{o} (Figure 6.16). The ratio of maximum shear

in the bone layer to that on the cartilage surface increased with the radius of the impact indenter (Table 6.1).

Table 6.1 Maximum shear stress and their ratio of shear in three cases

Indenter radius (mm)	Max. Shear in bone (MPa)	Max. Shear in cartilage (MPa)	Ratio of shear in bone to cartilage
2.0	4.048	2.821	1.435
4.0	5.351	3.163	1.679
20.0	7.544	3.712	2.032

The maximum tensile stresses were located on the edge of the impact indenter (Figure 6.17) and had magnitudes of 0.6 to 0.1 MPa for the three indenter cases. The maximum tensile strain was approximately 14.2%, 13.3%, and 10.2% in the 2.0, 4.0, and 20.0 mm indenter cases, respectively and it was located in the center of the contact zone directed parallel to the cartilage surface.

The shear stress distributions, τ_{xy}, are shown in Figure 6.18 for the three loading cases. In all cases, the maximum magnitude of τ_{xy} occurred at a distance from the symmetric line equal to approximately 60% of the radius of the contact area. The magnitudes of these maximum shear stresses were 1.6, 2.4 and 2.7 MPa in the 2.0, 4.0, and 20.0 mm indenter cases, respectively. The locations of these maximum shear values correlated very well with those found in the biphasic model of Ateshian (1994), who also obtained these values at a distance from the symmetric line equal to approximately 60 % of radius length of the contact area.

The Mises stresses distributions for the three models are shown in Figure 6.19 and are similar to the maximum shear stress distributions.

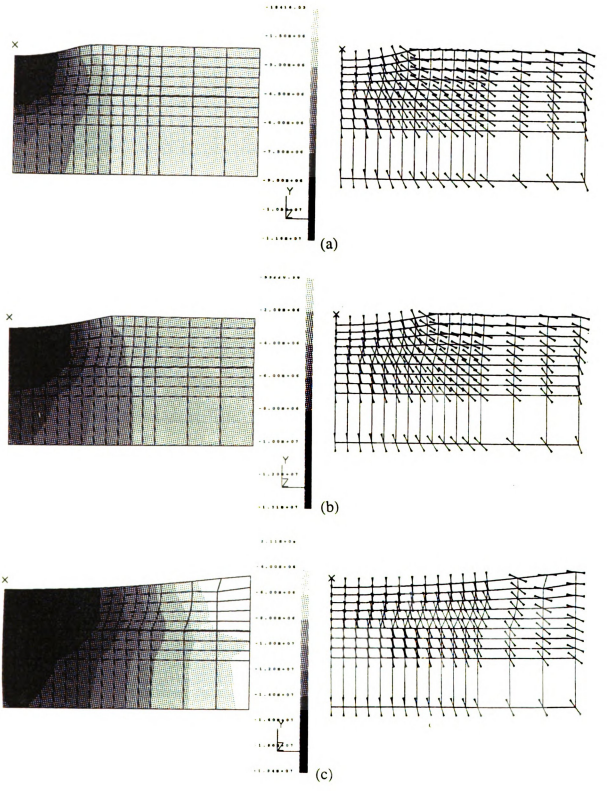

Figure 6.15 Minimum principal stresses and directions for the different indenters (Pa) (a) R=2.0 mm, (b) R=4.0 mm, and (c) R=20.0 mm.

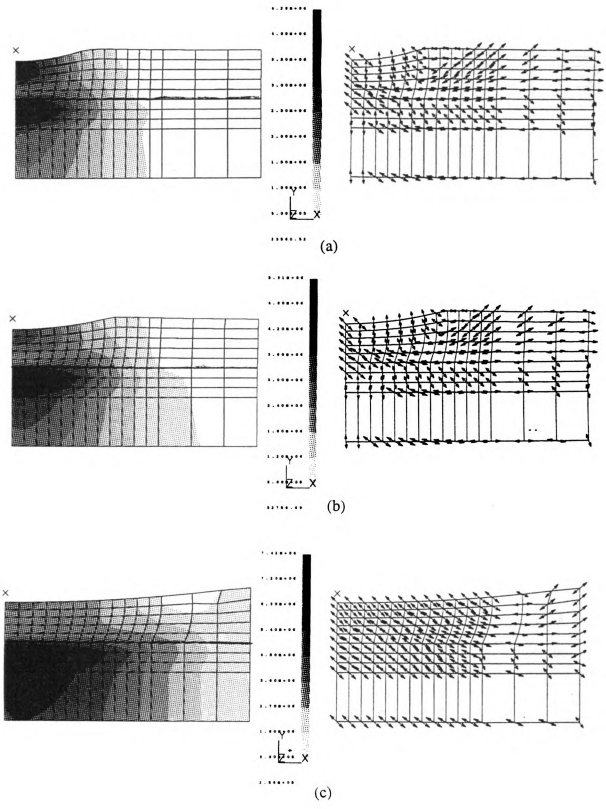

Figure 6.16 Maximum shear stresses and directions for the different indenters (a) R=2.0 mm, (b) R=4.0 mm, and (c) R=20.0 mm

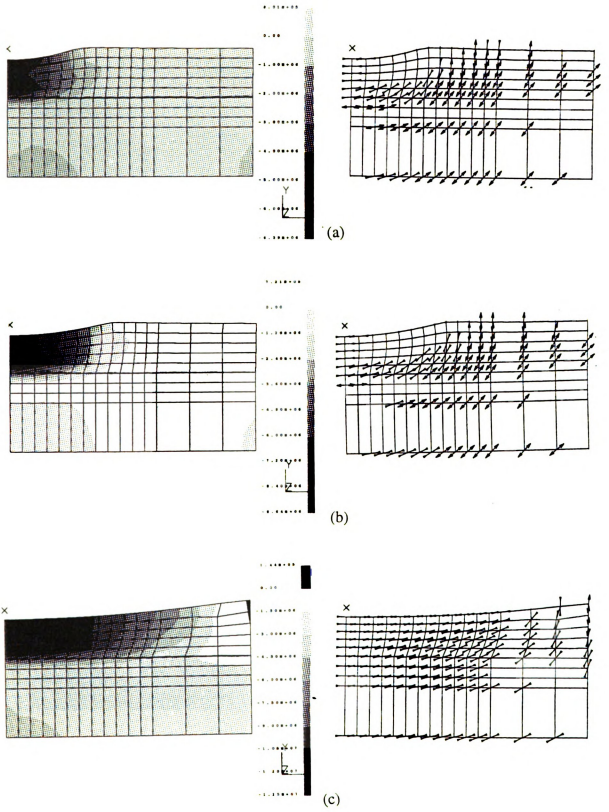

Figure 6.17 Maximum principal stresses and directions impacted by different indenters (a) R=2.0 mm, (b) R=4.0 mm, and (c) R=20.0 mm

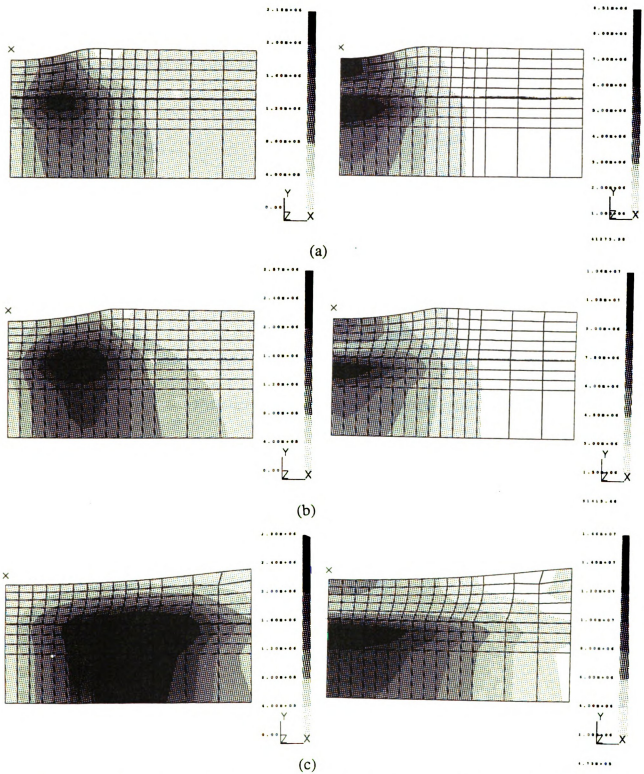

Figure 6.18 Shear stresses in the xy plane for different indenters (a) R=2.0 mm, (b) R=4.0 mm, and (c) R=20.0 mm

Figure 6.19 Mises' stresses for the different indenters (a) R=2.0 mm, (b) R=4.0 mm, and (c) R=20.0 mm

The maximum shear stresses at the top of the cartilage for the all cases are shown in Figure 6.20. Note that the shear stresses for the flattest indenter were 1.33 times higher than those caused by the small radius indenter.

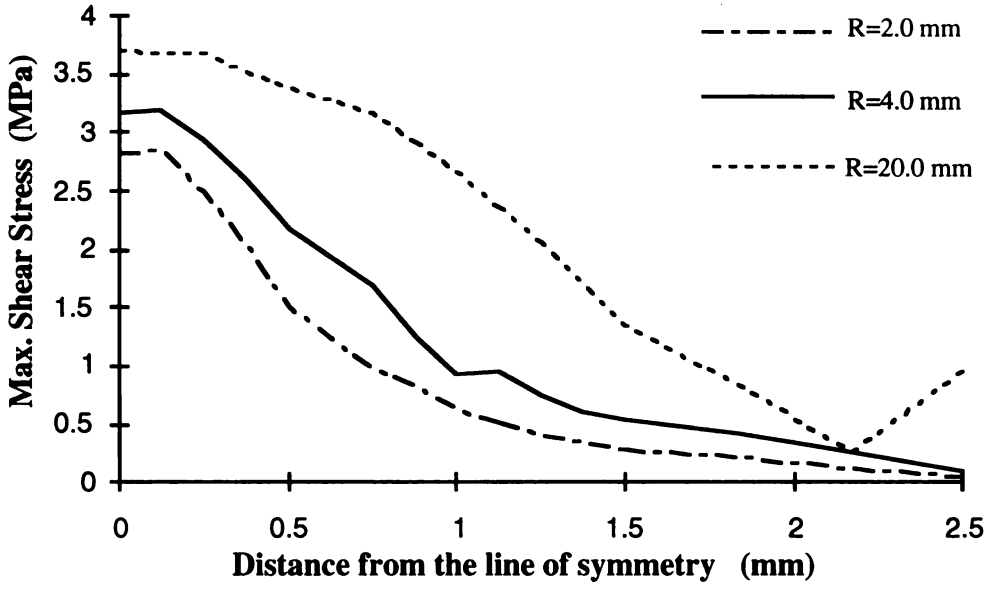

Figure 6.20 The distribution of maximum shear stresses at the top of the cartilage layer

The maximum shear stresses at the cartilage-bone interface are shown in Figure 6.21. The shear stresses generated for group 3 indenters were 1.79 times higher than those generated in test using the smallest radius indenter.

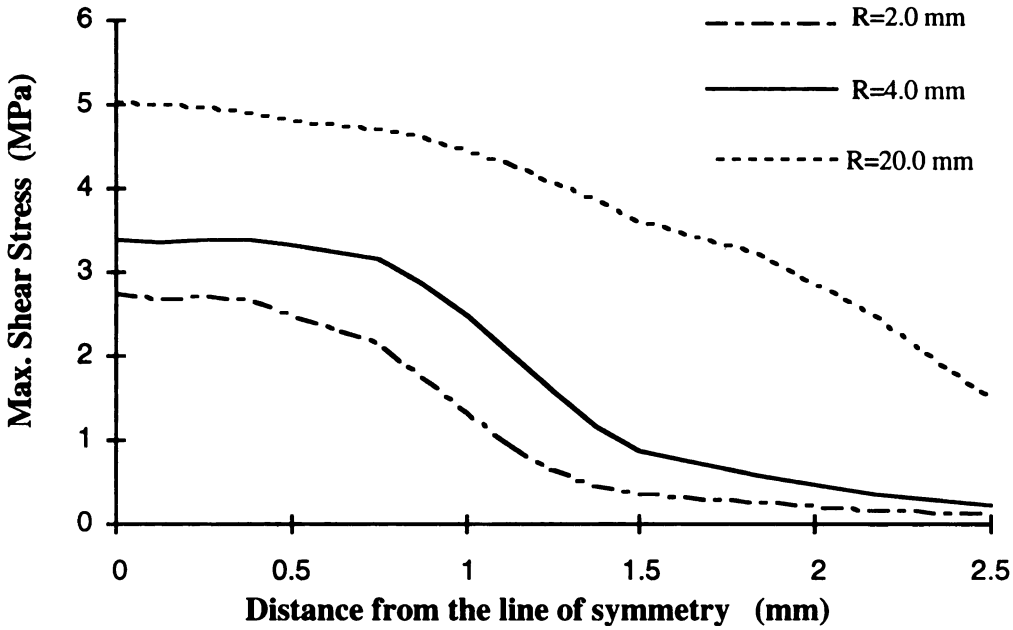

Figure 6.21 The distribution of maximum shear stresses at the interface between cartilage and bone for various indenters

The maximum shear stresses in the layer of bone just below the cartilage-bone interface are shown in Figure 6.22. The shear stresses resulting for impact the indenter with the largest radius were 1.88 times higher than those used by smallest radius indenter. The highest shear stress was 7.79 MPa, which may help explain the incident of bone damage in these experiments.

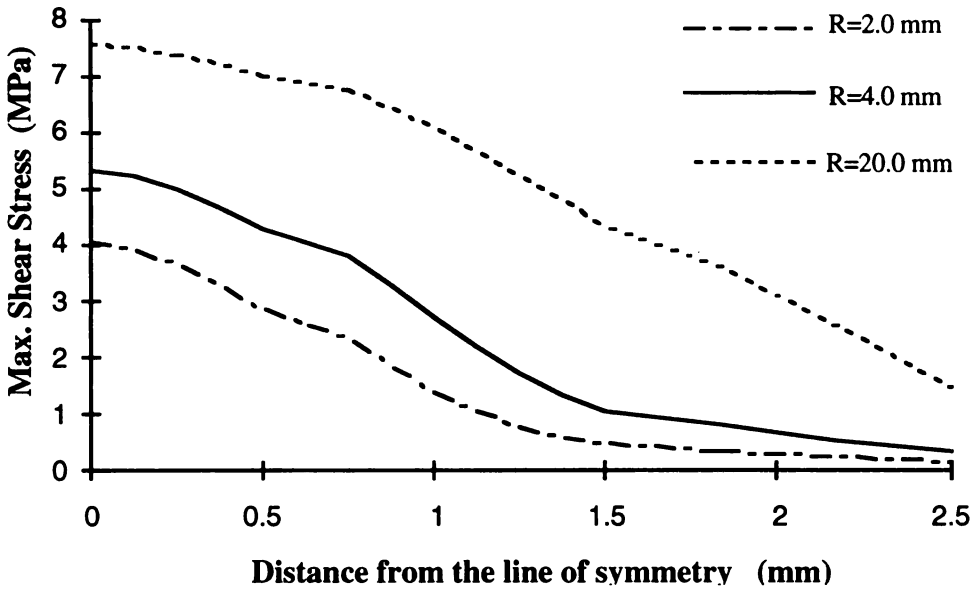

Figure 6.22 The distribution of maximum shear stress in the bone just below the cartilage-bone interface

6.3 A Coulomb-Mohr Failure Envelop for the Rabbit Tibial Cartilage

In Section 6.1, the locations of damage and the critical impact loads were described for the experiments. In the Section 6.2, the stress fields for these critical loads were determined by an axisymmetric FEM model. In this Section, a failure criterion has been developed to explain the mechanical cartilage damage.

By comparing the stress fields of Section 6.2 with the experimental results of Section 6.1, I could determine the maximum shear stresses and the mean stresses at the fissure location for each case. In all cases, the location of fissuring was at the center of contact.

The Coulomb-Mohr's circles associated with the three critical load conditions are plotted in Figure 6.23. The center point and the radius for the Coulomb-Mohr's circles are the mean failure stress and the maximum failure shear stress, respectively. These were 7.02 MPa and 2.82 MPa for the 2.0 mm indenter case, 8.90 MPa and 3.16 MPa for the 4.0 mm indenter case, and 15.6 MPa and 3.712 MPa for the 20.0 mm indenter case.

The ultimate tensile stress of cartilage, as determined by H. Yamada (1970), has also been plotted in Figure 6.23. The ultimate tensile stress was 3.3 MPa. According to H. Yamada, the ultimate shear stress is 65% of the ultimate tensile stress. This circle is also plotted in Figure 6.23. A failure envelop was determined by linear curve fitting for these three cases. The equation for these data was

$$\tau = 2.2251 + 0.097692\sigma \qquad (6.1)$$

$$R^2 = 0.962 \qquad (6.1\ a)$$

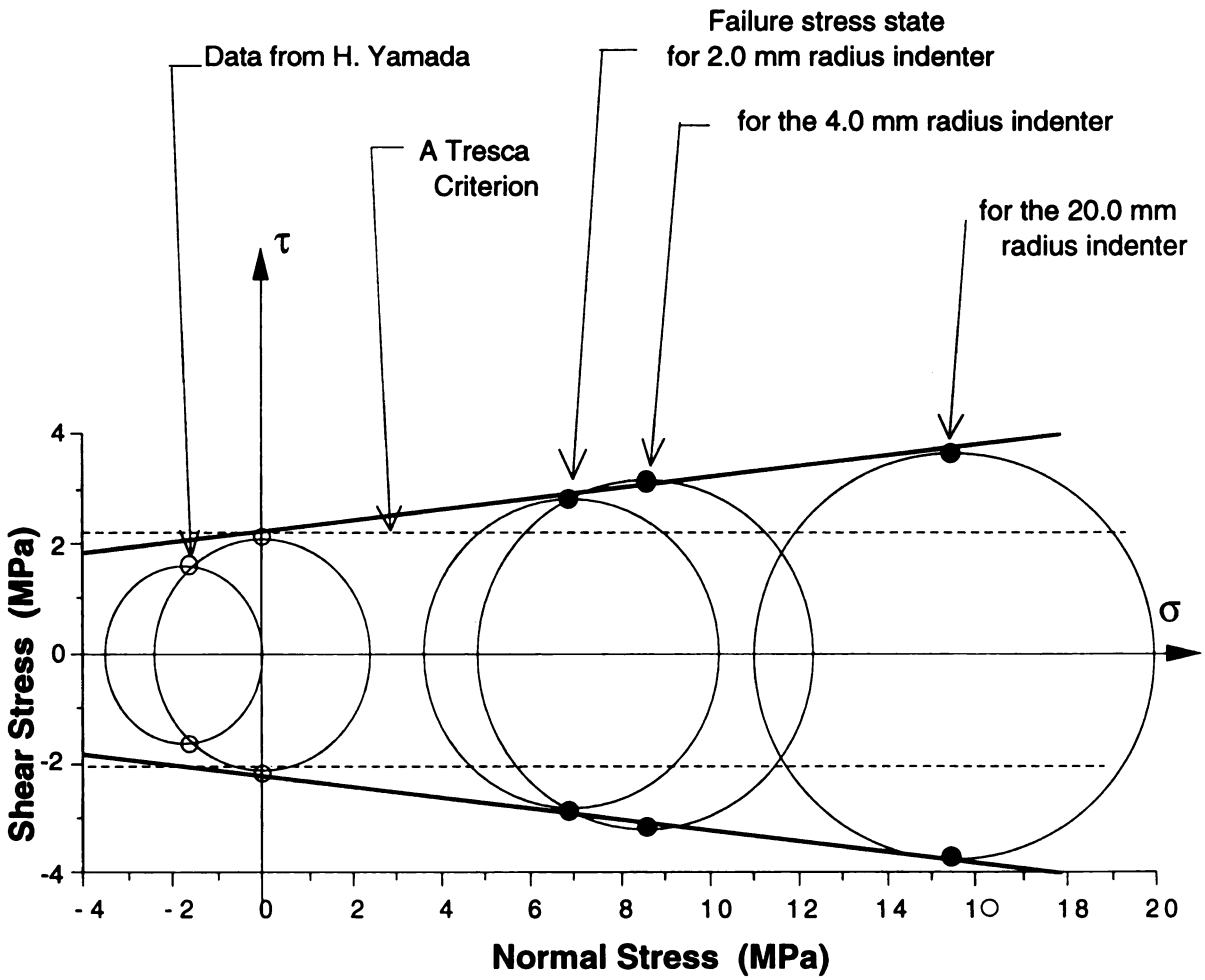

Figure 6.23 The failure envelop for tibial cartilage under impact loading

The failure envelop suggests that the failure shear stress increases with mean stress. Thus cartilage damage may be dependent upon two variables: the shear stress and the hydraulic pressure. A maximum shear stress theory, such as that suggested by Tresca, has also been shown in Figure 6.23 (dash line).

6.4 Application of the Criterion to Ide's Experimental Data

The experimental results from the thirty-four animals from Ide (1992) were outlined in Section 2.1. The corresponding stress analyses associated with these experiments were performed using the model of the patella described in Sections 5.1 and 5.2. In this Section, the failure criterion developed in Section 6.3 was applied to these data.

Cartilage damage always occurred on the lateral facet of the patella. The maximum shear stresses and mean stresses in that area was given in Table 5.1. Each pair of maximum shear stress and mean stress have been plotted in Figure 6.24 and 6.25. The solid dots represent those samples with observed fissures on the patellar cartilage surface, and the hollow dots represent those samples without fissures. The linear failure envelop developed from experiments on the tibial plateau has also been plotted in Figure 6.24. The non linear failure envelop developed from experiments and Yamada's data on the tibial plateau has been plotted in Figure 6.25. Note that most of the data associated with fissured specimens appear above or near the failure envelop. The non linear failure envelop shows better classification for these experimental data. A Tresca criterion, represented by the dashed line, would appear to be too conservative and not for the experimental data as well as the Coulomb-Mohr criterion.

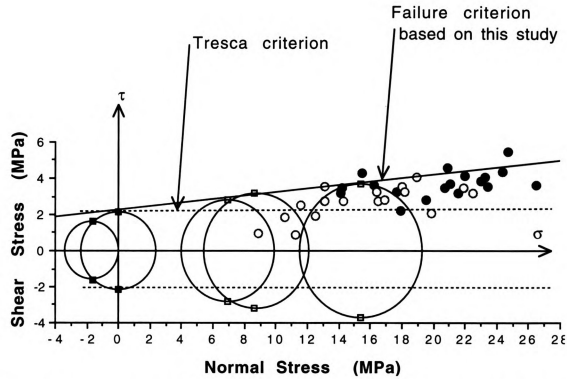

Figure 6.24 Application of the linear tibial failure criterion to Ide's data. Solid dot indicates a fissure, whole open circle indicates that no surface damage was observed experimentally by Ide.

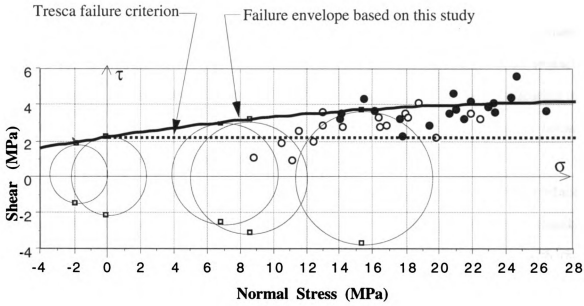

Figure 6.25 Application of the non linear tibial failure criterion to Ide's data. Solid dot indicates a fissure, whole open circle indicates that no surface damage was observed experimentally by Ide.

Chapter 7 Conclusions

The objective of the research in this dissertation was to develop a criterion to predict damage of articular cartilage caused by impact loading. A number of impact tests were performed on tibial plateaus to determine the critical states of initial damage. An axisymmetric finite element analysis model was set up to help document the distribution of the stresses and strains during blunt loading with various impact indenters. By comparing the damage location with the associated stress distribution, the correlated maximum shear stresses and the normal stresses in all three cases were used to develop a failure criterion. The failure envelop was a function of normal stress and maximum shear stress. It had been proposed that both maximum shear stress and hydraulic pressure affect fissure creation and the effect of hydraulic pressure can not be ignored. That is, the maximum shear stresses associated with the initial damage of cartilage are not a constant. Thus, a Tresca criterion is not applicable for the damage of cartilage during blunt impact. The criterion is robust and can be applied to other experimental data. The application of the failure criterion to Ide's experimental data shows a good ability to predict initial damage of cartilage during blunt impact on the bone.

In our indenter impact tests, most damaged specimens showed initial surface injuries at the center of the contact zone, and fissures (splits) were oriented approximately either 40 or 90^{o} to the cartilage surface. Comparing the zone of damage with the correlated stress field from the FEM model, I found that the maximum values of the maximum shear stresses occurred in the observed damage area, and the fissures were oriented parallel to the directions of maximum shear stresses. So I believe the initial fissures on the cartilage surface were due to excessive shear stress yet, the actual critical

stresses may be influenced by the properties used for the cartilage on the tibial plateau, which were actually taken from studies in patella cartilage. A few experimental observations are in agreement with my experimental observations (Repo, 1977; Broom, 1986; Haut, 1986; Thompson, 1990; Silyn-Roberts, 1990; Ide, 1990; Thompson, et al 1990; Tomatsu, 1992; Thompson, 1993). Repo and Finally (1977) documented radial fissures of human cartilage in the center of the contact zone at the cartilage surface extending to the deep zone, and death of chondrocytes when average normal contact pressures reached 25 MPa. Silyn-Roberts, et al, (1990) reported that impact induced failures of cartilage, in vitro, were usually in the center of the contact zone and oriented at 45 degrees to the articular surface and extended into the middle zone. They did not study the stress distribution inside the cartilage, but their experimental observation supports our results.

A few stress and strain analyses of the joint (Eberhardt, et al, 1990, Ateshian, 1994) show that the maximum shear stresses, τ_{xy}, are located at the bone cartilage interface away from the center of contact at 60 % of the contact radius. They suggest that the documented splits at the interface could be due to shear stress. Our solution also showed that the maximum values of τ_{xy} occurred in that location. But τ_{xy} is much smaller than τ_{max}. It is true, as we discussed in Section 1.2, there exits another type of damage phenomenon. The separation of the cartilage from the underlying bone in the zone of calcified cartilage has been reported in the previous model during blunt impact (Armstrong, 1982). Vener, et al, (1991) also observed cracks in the zone of calcified cartilage after impact of the canine joint. We also observed cracks at the interface in a few tests, but they occurred at the line of symmetry under the indenter and propagated along the tide mark in the calcified cartilage. When the tibia was impacted by a flat indenter, the FEM model showed two areas of the high shear stress: one at the contact surface, and one in the bone just below the cartilage-bone interface. My model results suggest that when the contact radii are large, such as in the human knee joint, there is a

possibility of initial damage occurring at the interface with bone versus the cartilage surface. On the other hand, we do not know the damage criterion and properties of calcified cartilage, per se. This is an area of future work.

This study suggested that the damage of cartilage on the tibial plateau due to blunt impact is controlled by two variables: shear stress and hydraulic pressure. In fact, the effect of static hydraulic pressure is significant and can not be ignored. So a Coulomb-Mohr damage criterion has been applied to study mechanics of biological tissue trauma. The difference between Coulomb-Mohr criterion and a Tresca theory is the effect of hydraulic pressure on material failure. There are three factors which could produce high hydraulic pressures in the articular cartilage of the knee joint. Firstly, a flat surface of articular cartilage and a low permeability would provide ideal conditions to keep the fluid inside and generate high hydraulic pressure during compressive loads. Secondly, if the loading occurs in a short time, the cartilage would generate a high hydraulic pressure because the water does not have time to move out. Thus, cartilage could bear very high loads without damage in this situation. The hydraulic pressure acts to help support the cartilage making it more resistant to shear damage. This may be the reason why the cartilage can withstand 3 or 4 times body weight during jumping and running, yet also be damaged simply by long periods of standing. Thirdly, the hydraulic pressure and shear stresses are affected by the directions of impact loading. The results in Appendix A showed that the contact pressures were uniform when impact was directed more centrally or a little more laterally in the rabbit model. In these cases, maximum values of shear stress at the interface of cartilage and bone were higher than those of shear stress at the cartilage surface. On the other hand, contact pressures were more bimodal when impact occurred on the medial side of the patella. In this case the maximum values of shear stress at the cartilage surface were higher than those at the interface of cartilage and bone. This may explain why surface damage was more prevalent in Ide's experiments. These results may be useful in the study of designs that could help prevent cartilage damage

during blunt impact. One must still develop a criterion for interface injuries of the cartilage.

Another important aspect of the work in this dissertation was to develop a method of estimating properties of the cartilage during impact tissues. An inverse method was employed to estimate the material properties of cartilage by comparing the distribution of experimental contact pressures to that generated by the FEM model. The residuals were minimized when Poisson's ratio was 0.49 for the layer of cartilage. This result was consistent with the biphasic model of Mow, et al (1980), and agreed with Eberhardt et al (1991) and Askew and Mow (1980) who selected values of 0.475 and 0.45, respectively, in their elastic models. In our study the difference between theory and experiment was also minimized when an elastic tensile modulus of 2 MPa was chosen for the layer of cartilage. In the joint model of Askew and Mow (1984), a value of 12 MPa was chosen for the analysis. Eberhardt et al (9) chose a value of 1.5 MPa for the elastic shear modulus of the cartilage (which corresponds to a tensile modulus of approximately 4.4 MPa if one assumes isotropy of the layer). The above discussion proposes that as a first order approximation, response of the rabbit joint under a blunt impact can be determined by assuming the layer of cartilage to be approximately incompressible, i.e. Poisson's ratio 0.49 with an elastic modulus of 2 MPa and a reasonable value of elastic modulus for the underlying bone. Since some of the experiments with the large radius indenter showed damage of cartilage in the zone of calcified cartilage, it will be necessary to develop a scheme to estimate properties of calcified cartilage and subchondral bone during impact. This is an area for future study that may have direct application to the human knee. A more complex description of joint tissues may give better estimates of the failure stress distributions. In the lower layers of cartilage and bone it may also be important to set up a three dimensional model of the knee for a better understanding of the effects of load direction and load location. This would be especially true for the human model, where transverse fractures of the patella are often observed (Shelp, et al, 1994). The current two

dimensional model can not show stress distributions in the z direction. Another area of future study would be to deal with the problem of stress waves developed during impact. Realistic impacts on the human knee during a car crash occur at speeds of 30 mph and higher. To study the stress distributions in cartilage and bone a dynamic FEM model would be necessary.

APPENDIX A The Effect of Loading Location on the Distribution of Stress and Strain in the Rabbit Knee joint

Stress analysis of the rabbit knee joint (X. Li, et al, 1993) suggested that the location of initial impact trauma may be dependent on the direction of the impacting load. A typical joint geometry was selected for calculating the effects of loading using the FEM model (Figure 4.4). The same input load was located at the three different sites on the anterior surface of patella; the medial side, the centers side and the lateral side, respectively. The contact pressures generated in the patello-femoral joint were calculated by the FEM model (Figure A.1). Loading on the more medial side of the anterior surface of patella (similar to the in vivo experiments of Ide) yielded a strong bimodal distribution of contact pressure. The contact pressures on the lateral facet were higher than those on the medial facet. When loading was on the center of the patella or the lateral side of the patella, contact pressures on the medial facet were higher than those on the lateral facet.

The location of loading affected the patello-femoral contact pressures and the resulting stress field. The maximum values of maximum shear for the three loading locations are listed in Table A.1. For loads acting on the medial facet of the patella (most of Ide's experiments) the highest shear stresses occurred on the cartilage surface. In this case the ratio of shear stress in the bone layer to that in the cartilage was 1.21. When loading acted on the center or the lateral facet, the ratio of the shear stress in the bone layer to the cartilage was up to 3.0 and 3.47 times, respectively. In Ide's experiments most impacts were directed in the more medial facet of the patella. The above results help explain why the mechanism of injury was surface fissures on the cartilage, without fracture of the calcified cartilage or underlying subchondral bone (Haut, 1991).

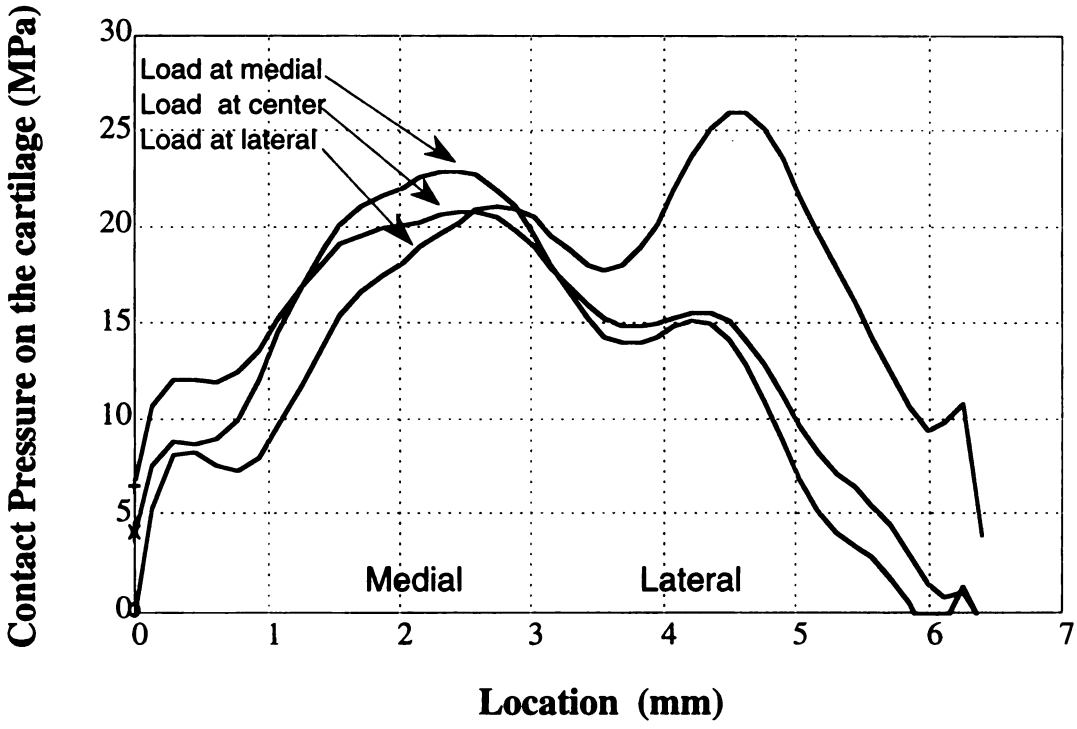

Figure A.1 This figure shows the effect of impact location on the distribution of contact pressures generated in the PF joint. More bimodal types of distributions were generated with more medial and lateral oriented impacts on the patella. A central located impact on the patella generated a more uniform profile of contact pressures over the medial and lateral facets.

Table A.1 Maximum shear Stress caused by different loading locations

Model Name	Load direction	Max. shear in subchondral bone (MPa)	Max. shear In cartilage surface (MPa)	Ratio of shear in the subchondral bone/cartilage
#3-medial	medial	6.0	5.76	1.21
#3-center	center	7.5	2.50	3.00
#3-lateral	lateral	8.0	2.88	3.47

APPENDIX B Estimation of Material Properties and Stress Analysis for the Human Knee Joint

(1) The FEM Model

The methods for the human knee joint experiments were discussed by Shelp (1994). The basic assumptions used in the human knee joint FEM model were essentially the same as for the rabbit FEM model (discussed in Chapter 3). The geometry for the 2 dimensional FEM model of the human knee joint was set up by sectioning one of the experimental samples and photographing its cross-section (Figure B.1). The section was located between two pin holes at a location coinciding with the zone of high contact pressure generated during impact (Figure B.2).

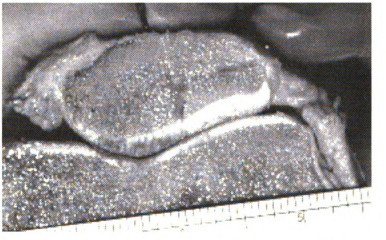

Figure B.1 The cross section of the human knee joint

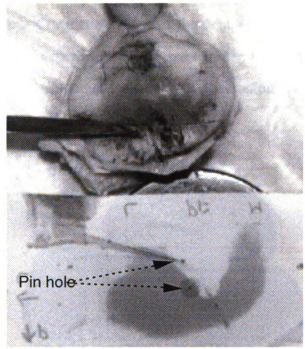

Figure B.2 A typical patella from the human knee joint and the corresponding Fuji film. The scalpel locates the location of the cross-section used for the FEM model.

Based on the geometry of the human knee joint shown in Figure B.1, an elastic finite element model was developed. For simplicity, a two dimensional analysis was performed with plane strain conditions assumed in order to represent a confinement of the cross section. The patella and distal femur were modeled with 3000 elements (See Figure B.3). Approximately 100 node-to-node gap elements were used to model the contact zone between the patellar and femoral cartilage surfaces. These were used in my assumption that no friction existed between contact surfaces on the patella and the femur during impacted loading.

The distal end of the femur was fixed at an unspecified distance from the patello-femoral joint, but the length was chosen to be quite removed from the joint proper. As in the animal model, the impact loading was applied to the human model based on the experimental pressure data from the anterior surface of the patella. Contact pressures

generated at the interface of the patella and the femur were measured in experiments with pressure sensitive film. Correlation between the contact pressures obtained from the model and those from the experiments were used to determine material properties of the cartilage using the inverse method discussed in this dissertation.

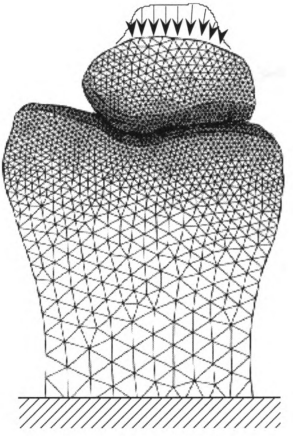

Figure B.3 FEM model of human knee joint

(2) Estimation of the Material Properties

The degree of correlation between the experimental and theoretical contact pressures in the PF joint depended on the material properties chosen for the cartilage. The calculated results from experiments Knee-1 and Knee-2, using the method of minimum residuals, are shown in Figures B.4 to B.7. As the value of Poisson's ratio

approached 0.475 for the cartilage, the residuals decreased (Figure B.4. and B.5). We also noted that the residuals were a minimum for an elastic modulus of the cartilage of approximately 1 to 2 MPa and a Poisson's ratio of 0.475 (Figure B.6 and B.7).

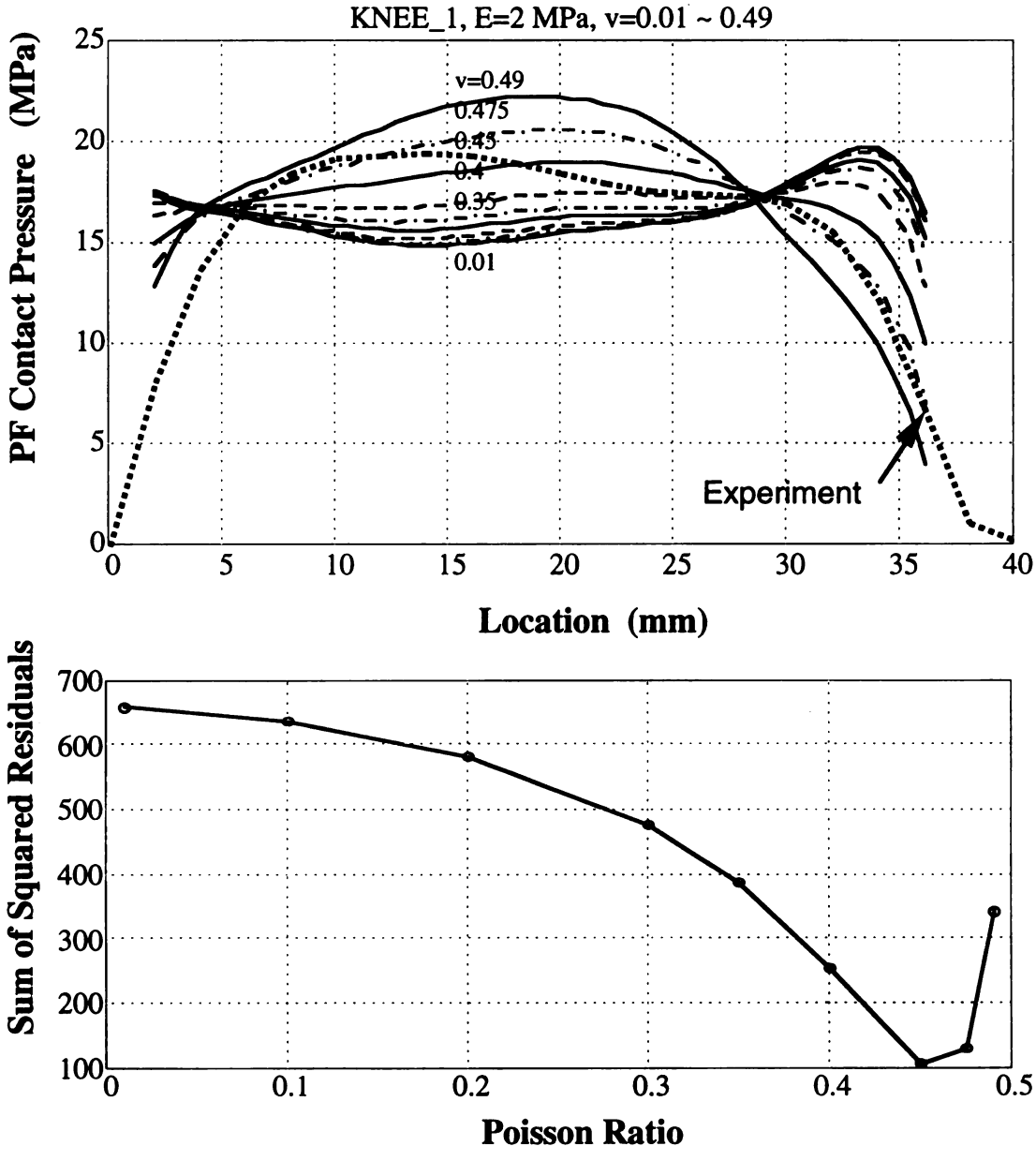

Figure B.4 (a) A plot showing the experimental contact pressure distribution and corresponding theoretical distributions for various values of Poisson's ratio in Knee-1 model. Note how well the results at 0.45 compare to the results from the experiments. (b) The residuals decreased continuously as Poisson's ratio approached 0.45.

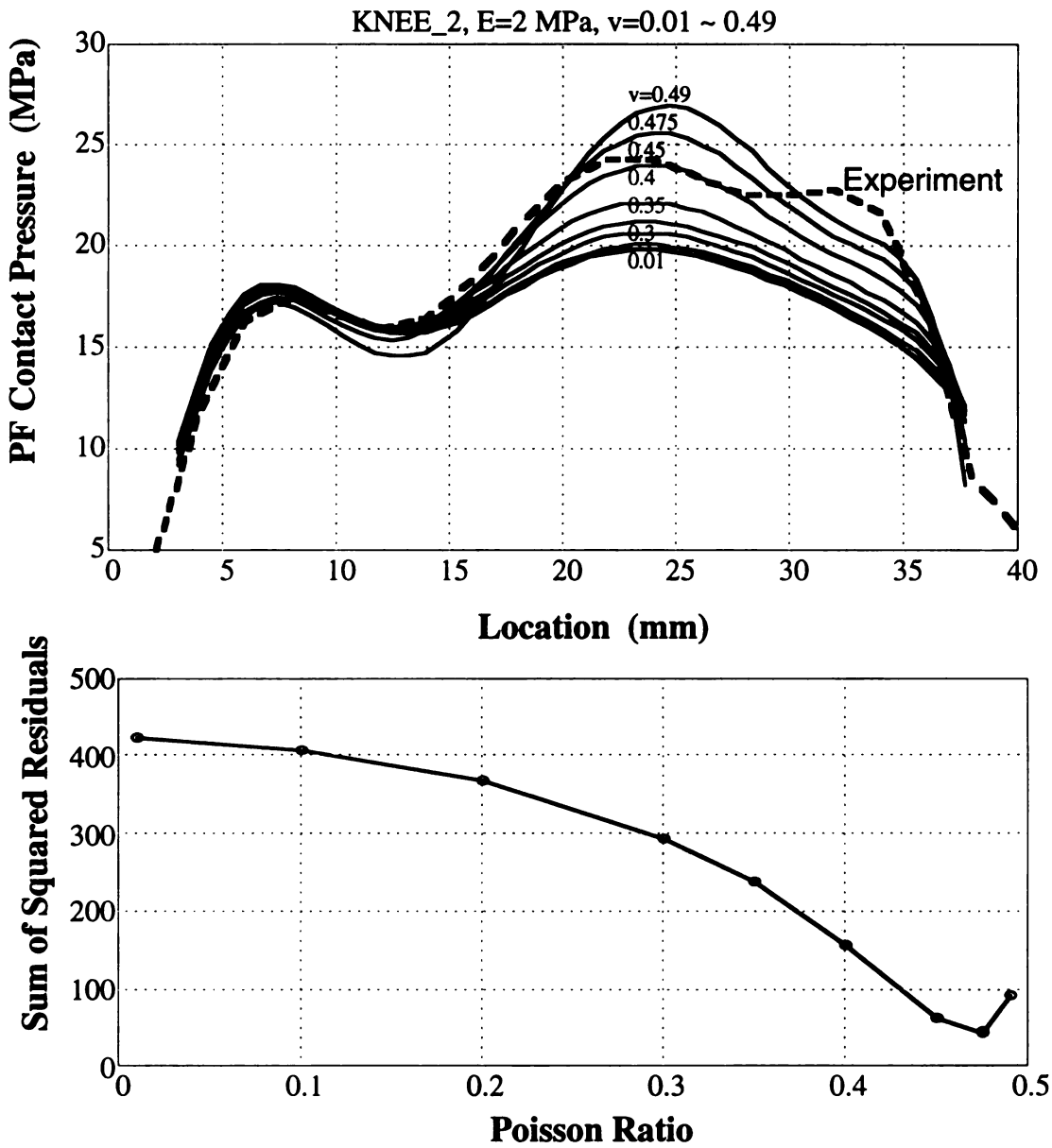

Figure B.5 (a) A plot showing the experimental contact pressure distribution and corresponding theoretical distributions for various values of Poisson's ratio in Knee-2 model. Note how well the results at 0.475 compare to the results from experiments. (b) The residuals decreased continuously as Poisson's ratio approached 0.475.

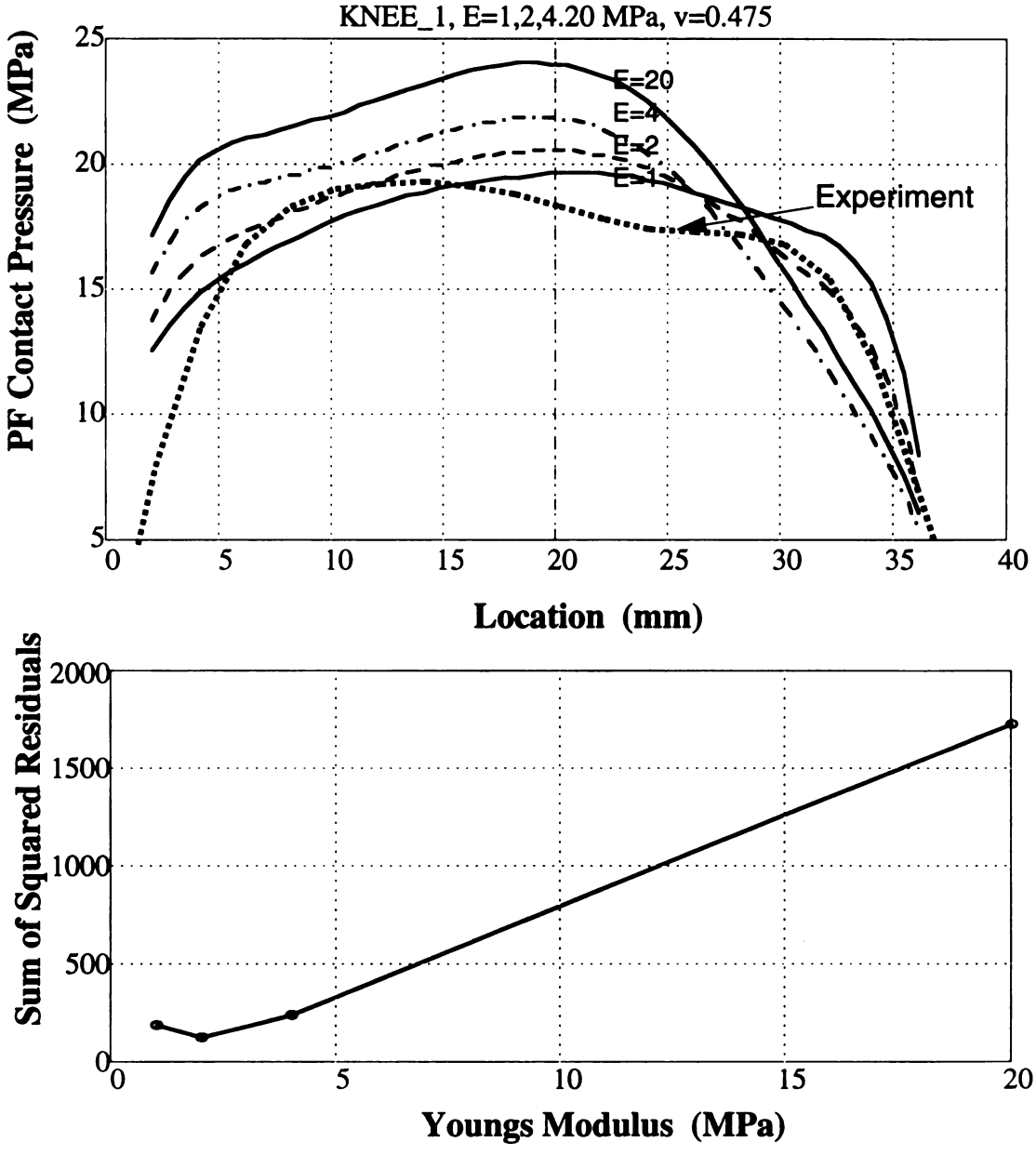

Figure B.6 (a) The effect of variations in the elastic modulus of cartilage on the residuals computed between the experimental and the theoretical contact pressures. A minimum was obtained for an elastic modulus near 2 MPa for the cartilage at Poisson's ratio less than 0.475 in Knee-1 model. (b) This plot shows the residuals for Young's modulus from 1 to 20 MPa.

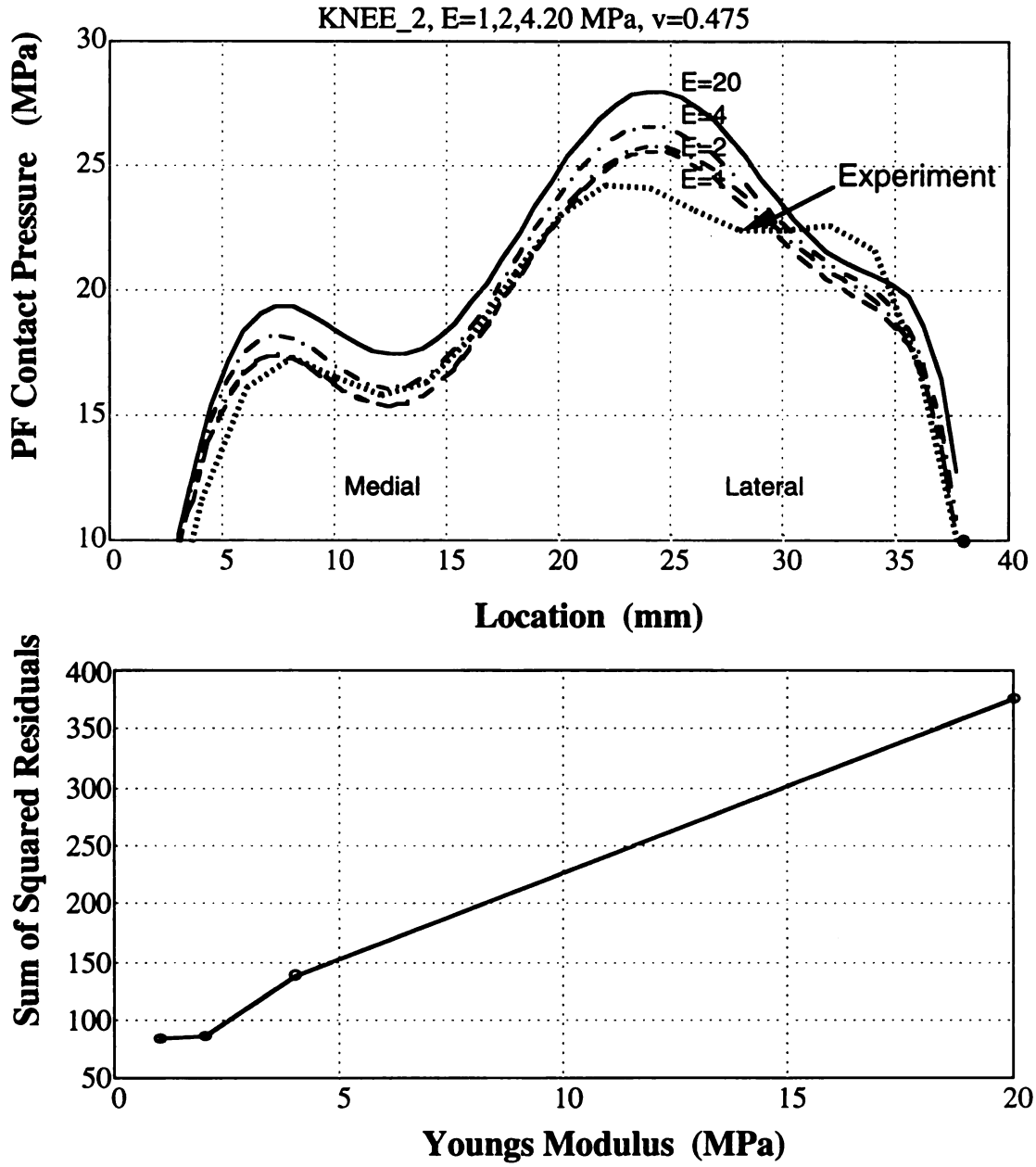

Figure B.7 (a) The effect of variations in the elastic modulus of cartilage on the residuals computed between the experimental and the theoretical contact pressures. A minimum was obtained for an elastic modulus near 2 MPa for the cartilage at Poisson's ratio less than 0.475 in Knee-2 model. (b) This plot shows the residuals for Young's modulus from 1 to 20 MPa.

(3) The Stress Distribution in the Human Knee Joint

Using these optimized values for the material properties of the cartilage and the contact pressures measured experimentally on the anterior surface of patella , I obtained the stress distributions from the FEM knee joint model. The contour plots of the minimum principal stresses and the maximum shear stresses in the knee joint model (Knee-2) are shown in Figures B.8. There were two areas of high shear stress in the knee joint; one at the cartilage surface and another at the subchondral bone layer. The maximum shear stresses developed within the subchondral bone were 23 MPa in the knee-2 model and 12 MPa in knee-1 model, respectively. The maximum shear stresses developed on the cartilage surface were 5.9 MPa and 5.7 MPa, respectively.

The distributions of the maximum shear stresses and the minimum principal stresses for the Knee-2 FEM model are plotted in Figure B.8. Since the surfaces of cartilage in both knee joints were fissured or damaged before impact, we could not tell if impact loading caused surface damage. (See a typical human cartilage in Figure B.2). But in some experiments reported by Haut, et al, (1994) cracks were observed lying in the subchondral bone.

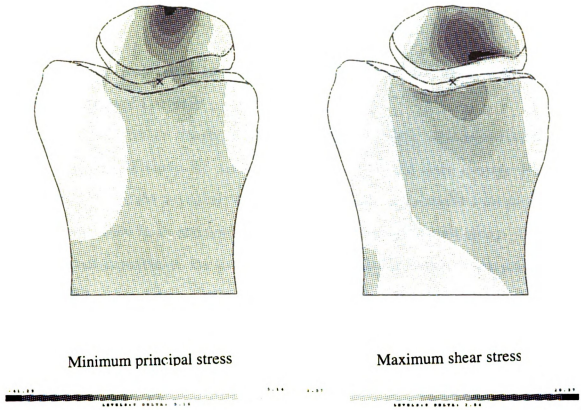

Figure B.8 The contour plots of the minimum principal stress and the maximum shear stresses in the Knee-1 model

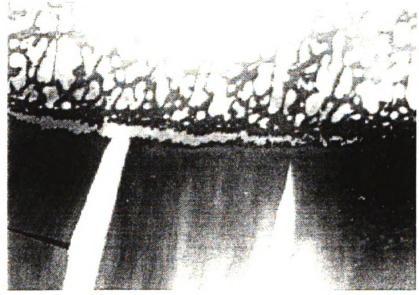

Figure B.9 Crack propagation along subchondral bone in the typical section of human knee patella (Knee-2 specimen).

APPENDIX C Application of the Coulomb-Mohr Criterion to Human Knee Joint

(1) The Damage of Cartilage

A total of fifteen human knee joint impact tests were performed (Haut, et al, 1994). In order to study the mechanisms of cartilage and bone damage for these experiments, I used the previously discussed FEM model, and examined the distribution of stress and strain in an attempt to correlate these parameters with injury. For these fifteen impact experiments, the contact loads on the anterior surface of the patella were not recorded. Therefore, the FEM model used to analyze these experiments had to be changed. In order to study the distribution of stress and strain in the patella, I used the measured contact pressures in the patello-femoral joint as the input loading boundary conditions (C.1).

The geometry for the 2-dimensional finite element model used for modeling these experiments was taken from specimen knee-2. The FEM model was constructed using 1300 plane strain elements (Figure C.1). The Young's modulus and Poisson's ratio for bone were assumed to be 2 GPa and 0.3, respectively (Cowin, S., 1987). The Young's modulus and Poisson's ratio for cartilage were assumed to be 2.0 MPa and 0.475, respectively. The values were obtained by the inverse method discussed in Appendix B

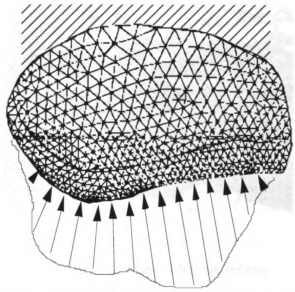

Figure C.1 The 2-D patellar FEM model for the human data analysis of the boundary conditions

The contact pressure profiles measured from the Fuji film (Figure B.2) were used as the input boundary conditions at the cartilage surface (Figure C.1). The contact pressure distribution was documented across the lateral and medial facets of the patella by taking a 0.5 mm thick slice of the distribution and generating a 2-dimensional pressure profile. The anterior aspect of the patella was rigidly fixed (Figure C.1). From these experimental data, fifteen different input loads were used in the FEM model to obtain the related stress fields.

Analyzed by the human FEM model, the maximum shear stresses and mean stresses on the cartilage surfaces were obtained. Since cartilage surfaces were fissured or damaged before impacted for all specimens due to pre-existing pathology, I could not tell if the impact loading caused damage, (See a typical human cartilage in Figure C.2). The maximum shear and mean stresses are plotted in Figure C.3 for these experiments. The Coulomb-Mohr criterion for the rabbit is also plotted. It is clear that most of human data lies below the failure envelope developed from the rabbit experiments. Maybe the flat contact surfaces in the human knee joint and the center impact loading produced higher stress in the bone, and produced the microcracks shown in Figure C.2.

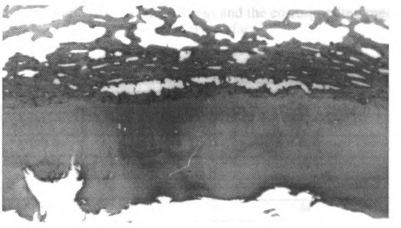

Figure C 2 Cartilage damage of human patella

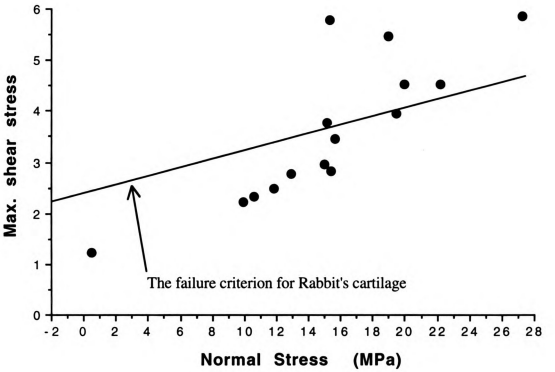

Figure C.3 Application of Coulomb-Mohr criterion to the human cartilage data

Table C.1 The maximum values of shear stress and the corresponding mean stresses on the cartilage surface

Exp. Name	Mean Stress (MPa)	Max. Shear Stress (MPa)
ho2-ro3	10.57	2.32
9793-r5	15.16	3.78
9793-l1	18.94	5.49
8093-r1	12.93	2.78
8093-l5	27.29	5.88
7093-l1	15.43	2.84
6893-r1	0.46	1.22
6893-l4	11.87	2.49
4393-l2	15.64	3.45
28091-le	14.99	2.96
26993-r1	20	4.53
26993-l5	19.44	3.96
1021-r6	22.21	4.52
1021-l1	9.91	2.24
7093-knee-2	15.31	5.79

(2) The Damage of Subchondral Bone

The FEM model has been utilized to study the bone damages reported in Table C.2. By using the human patellar FEM model and the 15 different pressure distributions as input, the stress distributions in the patella were obtained. The maximum shear stress and the mean stress in the bone just below the cartilage-bone interface (in the subchondral bone layer) are plotted in Figure C.4. The solid dots represent the samples with subchondral bone cracked, and the hollow dots represent those with no damage observed by experiment. We found eight out of fifteen specimens had cracks in the subchondral bone. A typical crack is shown in Figure C.5. Since I could not find any information about the ultimate tensile or compression stress for human subchondral bone, I could not develop a failure envelope. However these experimental data do show an increasing state of hydrostatic stress as shear stress increases in the subchondral bone. Hence, I could imagine that both parameters will be involved in any future criterion developed for

subchondral bone.

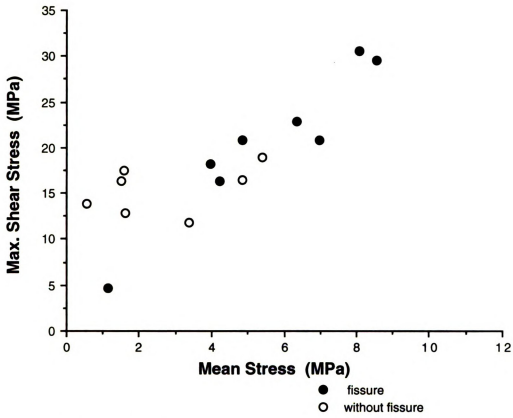

Figure C.4 Results of the stress analysis in the subchondral bone for the fifteen human knee joint experiments

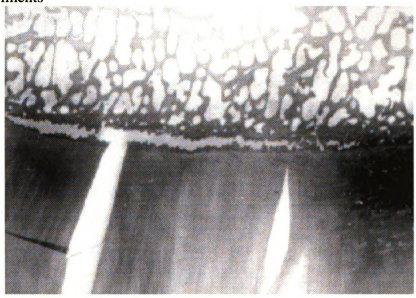

Figure C.5 Crack propagation along subchondral bone in this typical section of human patella

Table C.2 Experimental observation and data

Test No.	Crack in subchondral bone	Mean Stress (MPa)	Max. Shear Stress (MPa)
ho2-ro3	no	1.61	12.88
9793-r5	no	0.56	13.90
9793-l1	no	1.50	16.35
8093-r1	yes-center	4.22	16.29
8093-l5	yes	8.07	30.57
7093-l1	yes-center	6.96	20.84
6893-r1	yes-medial	1.14	4.63
6893-l4	no	4.84	16.43
4393-l2	no	1.60	17.47
28091-le	no	5.40	18.95
26993-r1	yes	3.98	18.16
26993-l5	yes	4.86	20.83
1021-r6	yes	8.55	29.55
1021-l1	no	3.37	11.79
7093-5	yes	6.34	22.92

BIBLIOGRAPHY

Altiero, N. J., Fracture Initiation and Propagation in Nonuniform Compressive Stress Fields, Ph.D. dissertation, University of Michigan, (1974).

Armstrong, C. G., Lai, W. M., and Mow, V. C., An Analysis of the Unconfined Compression of Articular Cartilage, ASME Journal of Biomechanical Engineering, Vol. 106, (1984), pp165-173.

Askew, M. and Mow, V., The Biomechanical Function of The Collagen Fibril Ultrastructure of Articular Cartilage, Journal of Biomechanical Engineering, Vol. 100, (1978), pp105-115.

Ateshian, G. A., Lai, W. M., Zhu, W. B. and Mow, V. C., An Ansysptotic Solution for The Contact of Two Biphasic Cartilage Layers, Journal of Biomechanics, Vol. 27, (1994), pp1347-1360.

Blankevoort, L., Kuiper, J. H., Huiskes, R. and Grootenboer, H. J., Articular Contact in a Three-Dimensional Model of The Knee, Journal of Biomechanics, Vol. 24, (1991), pp1019-1031.

Brown, P., Sorrells, R., Kovaleski, T. and Maloney, F., Interdisciplinary Approach to Arthritis Rehabilitation, Journal Arkansas Medical Society, (1988), pp474-476.

Chapchal, G., Posttraumatic Osteoarthritis after Injury of The Knee and Hip Joint,. Reconst. Surg. Trauma, Vol. 16, (1978), pp87-94.

Chin, M., Donahue, J., Erdman, A., Oegema, T. and Thompson, R., Biomechanical Analysis of an Adult Canine Patella under an Indirect Blunt Trauma, Proceedings of the 32nd Annual Meeting of ORS., (1986).

Clark, D. L., Surface Characteristics of Human Articular Cartilage-a Scanning Electron Microscope Study, Journal of Anatomy, Vol. 108, (1971).

Clark, J., The Organization of Collagen Fibrils in The Superficial Zones of Articular Cartilage, Journal of Anatomy, Vol. 171, (1990), pp117-130.

Cowin, S., Van Buskirk, W. and Ashman, R., Properties of Bone Handbook of Bioengineering, Chapter 2, (1987), pp2-27.

Donahue, J. M., Buss, D., Oegema, T. R. and Thompson, R. C., The Effects of Indirect Blunt Trauma on Adult Canine Articular Cartilage, Journal of Bone and Joint Surgery, Vol. 65(A), (1983), pp948-957.

Eberhardt, A. W., Lewis, J. L., Keer, L. M. and Vithoontien, V., An Analytical Model of Joint Contact, Journal of Biomechanical Engineering, Vol., 112, (1990), pp407.

Eberhardt, A., Lewis, J. and Keer, L., Normal Contact of Elastic Spheres with Two Elastic Layers as a Model of Joint Articulation, Journal of Biomechanical Engineering, Vol. 113, (1991), pp410-417.

Fung, Y. C., Foundations of Solid Mechanics, Prentice Hall, Inc., 1965, pp20-28.

Hale, J. E., and Brown, T. D., Contact Stress Gradient Detection Limits of Pressensor Film, Journal of Biomechanical Engineering, Vol. 114, (1992), pp352-357.

Haut, R. C., Contact Pressures in the Patello-Femoral Joint During Impact Loading on The Human Flexed Knee, Journal of Orthopedic Research, Vol.7, (1989), pp272-280.

Haut, R. C., The Influence of Superficial Tissue on Response of the Primate Knee to Traumatic Posterior Tibia Drawer, Journal of Biomechanics, Vol. 16, (1983), pp465-472.

Haut, R. C., Impact Studies on The Canine Knee Model, Proceedings of American Society of Biomechanics, Vol. 9, (1985), pp117-118.

Haut, R. C., Ide, T. M., Walsh, J. C., Robbins, J. L. and DeCamp, C. W., Studies on The Blunt Impact Response of Articular Cartilage: Animal Experiments, Human Cadaver Experiments, and Mathematical Modeling, Proceedings of the Second Symposium. on Injury Prevention Through Biomechanics CDC, (1992), pp21-40,.

Haut, R. C., Shelp, D., Li, X., and Altiero, N. J., Studies on the Impact Response of Articular Cartilage to Blunt Impact, Injury Prevention Through Biomechanics: Symposium Proceedings CDC, (1993), pp177-200.

Hayes, W. and Keer, L., Herrmann, G. and Mockros, L., A Mathematical Analysis for Identification Tests of Articular Cartilage, Journal of Biomechanics, Vol. 5, (1972), pp541-551.

Heather Silyn-Robberts, Fracture Behavior of Cartilage-on-Bone in Response to Repeated Impact Loading, Connective Tissue Research, Vol. 24, (1990), pp41.

Hirsch, C., A Contribution to the Pathogenesis of Chondromatacia of Patella, Acta Chirurgica Scandinavica Supplementum, Vol. 83, (1944), pp1-106.

Huberti, H., Hayes, W. and Stone, J., Determination of Patello-Femoral Contact Stresses Using Pressure Sensitive Film, Proceedings of the 10th Annual Meeting of Northeast Bioengineerng Conference, Vol. 10, (1982), pp1-4.

Ide, T. M., An Analysis of Impact-Induced Trauma to Articular Cartilage, Thesis, Michigan state university, 1992.

Insall, J., Falvo, K. A. and Wise, D. W., Chondromalacia Patellae: a Prospective Study, Journal of Bone and Joint Surgery, Vol. 58, (1976), pp1-8.

Jurvelin, J., Kivironta, I., Saamanen, A. M., Tammi, M. and Helminen, H. J., Indentation Stiffness of Young Canine Knee Articular Cartilage- Influence of Strenuous Joint Loading, Journal of Biomechanics, Vol. 23, (1990), pp1239-1246.

Mankin, J., Current Concepts Review: The Response of Articular Cartilage to Mechanical Injury, Journal of Bone and Joint Surgery, Vol. 64, (1982), pp460-466.

Meachim, G. and Bentley, G., Horizontal Splitting in Patellar Articular Cartilage, Arthritis Rheumatism, Vol. 21, (1978), pp669-674.

Meachim, G., and Brooke, G., Osteoarthritis: Diagnosis and Management, eds., R. W. Moskowitz et al., W. B. Saunders Co., Phila. Pa., (1984), pp29-42.

Mente, P. and Lewis, J., Elastic Modulus of Calcified Cartilage, Proceedings of the 38th Annual. Meeting of ORS, Vol. 38, (1992), pp212.

Minns, R. J., Birnie, A. J. M. and Abernethy, P.J.A, Stress Analysis of The Patella, and How It Relates to Patellar Articular Cartilage Lesions. Journal of Biomechanics, Vol. 12, (1979), pp699-711.

Mow, V. C., Lai, W. M. and Redle, I., Some Surface Characteristics of Articular Cartilage, Part I: A Scanning Electron Microscopy Study and a Theoretical Model for the Dynamic Interaction of Synovial Fluid and Articular Cartilage, Journal of Biomechanics, Vol. 7, (1974), pp449.

Mow, V. C., Kuei, S., Lai, W. and Armstrong, C. G., Biphasic Creep and Stress Relaxation of Articular Cartilage in Compression: Theory and Experiments, Journal of Biomechanical Engineering, Vol. 102, (1980), pp73-84.

Parsons, J. R. and Black, J., The Viscoelastic Shear Behavior of Normal Rabbit Articular Cartilage, Journal of Biomechanics, Vol. 10, (1977), pp21-19.

Radin, E., Ehrlich, M., Chernack, R., Abernethy, P., Paul, I. and Rose, R., Effect of Repetitive Impulsive Loading on the Knee Joints of Rabbits, Clinical Orthopedics and Related Research, Vol. 131, (1978), pp288-293.

Ratcliffe, A., Shuretry, W. and Caterson, B., The Quantitation of a Native Chondroitin Sulfate Epitope in Synovial Fluid Lavages and Articular Cartilage from Canine Experimental Osteoarthritis and Disuse Atrophy, Arthritis Rheumatics, Vol. 36, (1993), pp543-551.

Repo, R. and Finally, J., Survival of Articular Cartilage After Controlled Impact, Journal of Bone and Joint Surgery, Vol. 59, (1977), pp1068-1076.

Richard Skalak and Shu Chien, Handbook of Bioengineering, McGraw-Hill Company, 1987.

Schwartz, M. H., Leo, P. H. and Lewis, J. L., A Microstructural Model for the Elastic Response of Articular Cartilage, Journal of Biomechanics, Vol. 27, (1994), pp865-873.

Silyn-Roberts, H. and Broom, N., Fracture Behavior of Cartilage-on-Bone in Response to Repeated Impact Loading, Connective Tissue Research, Vol. 24, (1990), pp143-156.

Simon, B. R. and Woo, S. I-Y., A Relaxation and Creep Linear Viscoelastic Models for Normal Cartilage, ASME Journal of Biomechanical Engineering, Vol. 106, (1984), pp159-164.

Spilker, R. L, Jun-Kyo Suh and Van C. Mow, A Finite Element Analysis of the Indentation Stress-Relaxation Response of Linear Biphasic Articular Cartilage, Journal of Biomechanical Engineering, Vol. 114, (1992), pp191.

States, J., Traumatic Arthritis - A Medical and Legal Dilemma, Proceedings of the 14th Annual Conference of the American Association for Automotive Medicine, Vol. 14, (1970), pp21-28.

Tomatsu, T., et al, Experimentally Produced Fractures of Articular Cartilage and Bone, Journal Bone Joint surgery, Vol. 74B(3), (1992), pp457-462.

Thompson, R. C., Oegema, T. R., Lewis, J. L. and Wallace, L., Osteoarthritic Changes After Acute Transarticular Load, Journal of Bone and Joint Surgery, Vol. 73-A(7), (1991), pp990-1001.

Timoshenko, S. P. and Goodier, J. N., Theory of Elasticity, the third edition, McGraw-Hill, 1982.

Vener, M. J., Thompson, R. C., Lewis, J. L. and Oegema, T. R., Subchondral Damage After Acute Transarticular Loading - An in Vitro Model of Joint Injury, Journal of Orthopedics Research, Vol. 10, (1992), pp759-765.

Weiss, C., Rosenberg, L. and Helfet, A. J., An Ultrastructural Study of Normal Young Adult Human Articular, Journal of Bone and Joint Surgery, Vol. 50A, (1986), pp663.

Woo, S., Akeson, W. and Jemmott, L., Measurements of Nonhomogeneous, Directional Mechanical Properties of Articular Cartilage in Tension, Journal of Biomechanics, Vol. 9, (1976), pp785-791.

Wright, V., Post-Traumatic Osteoarthritis- A medico-legal minefield. British Journal of Rheumatics., Vol. 29, (1990), pp474-478.

Yamada, Hiroshi, Strength of Biological Materials, Edited by F. Gaynor Evans, (1970).


MICHIGAN STATE UNIV. LIBRARIES
31293015796000